Amphibole-plagioclase fractional crystallisation and magma mixing as major differentation processes in the Akrotiri Volcanic Complex, Santorini, Greece

Autor(en): **Gartzos, Eutheme / Dietrich, Volker J. / Davis, Eleventheria**

Objekttyp: **Article**

Zeitschrift: **Schweizerische mineralogische und petrographische Mitteilungen = Bulletin suisse de minéralogie et pétrographie**

Band (Jahr): **79 (1999)**

Heft 2

PDF erstellt am: **19.09.2024**

Persistenter Link: https://doi.org/10.5169/seals-60207

SCHWEIZ. MINERAL. PETROGR. MITT. 79, 231–262, 1999

Amphibole-plagioclase fractional crystallisation and magma mixing as major differentiation processes in the Akrotiri Volcanic Complex, Santorini, Greece

by *Eutheme Gartzos*[1], *Volker J. Dietrich*[2] and *Elevtheria Davis*[1]

Abstract

The Pleistocene Akrotiri Volcanic Complex (AVC) builds up the southern part of the island of Thera and comprises the oldest volcanic rocks of the Santorini volcanic islands with ages probably ranging from 1.6 to 0.5 Ma. The lower volcanic sequence starts mainly with rhyodacitic magmas, continuing with the production of heterogeneous dacites and terminating this first cycle with andesites.

The rhyodacitic magmas are results of fractional crystallisation of amphibole- and plagioclase-rich cumulates from a water-bearing basaltic melt with island arc characteristics. The andesitic to dacitic magmas, in contrast, are mainly products of mechanical mixing (mingling) between rhyodacitic and basaltic to andesitic melts. These differentiation processes can be inferred from phenocryst and xenocryst chemistry as well as from basic to intermediate inclusions, which occur in various proportions in the dacitic and rhyodacitic lavas. The inclusions are interpreted as undercooled and quenched ("pillowed") products, which were formed by injection of vapor-rich hybrid-melts of basaltic to andesitic composition into cooler dacitic to rhyodacitic magmas. Such injections are seen as trigger mechanism, which started the ascent of silicic magmas from deep-seated crustal magma reservoirs.

The upper and younger volcanic sequence of the AVC is composed of high-alumina basalts and basaltic andesites and erupted after a period of magmatic quiescence. Complete magma mixing is present in the late Pleistocene Cape Mavrorachidi eruptive centre, producing cinder, scoriae and lavas of basaltic andesite composition. Textural patterns and mineral chemistry of the larger phenocrysts (xenocrysts) exhibit significant evidence of magma mixing between an evolved andesitic melt and a basaltic melt.

Keywords: volcanism, magma mingling, magma mixing, fractional crystallisation, amphibole, magmatic inclusions, Akrotiri Volcanic Complex, Santorini.

1. Introduction

The islands of Santorini mark the central part of the south Aegean island arc which extends over a distance of approximately 500 km from Corinth in the Saronic Gulf bordering Attica and the Peloponnisos to the islands of Kos and Nisyros near the Turkish coast. The arc is regarded as a magmatic expression of the still-active subduction of the African plate beneath the Aegean plate, which started around 4 Ma at the beginning of Pliocene (FYTIKAS et al., 1976 and 1984).

The base of the volcanic arc rests on normal and partially thinned continental crust and underwent several stages of deformation and metamorphism during the Alpine orogeny from Cretaceous to Late Tertiary. The main volcanic fields in the central and eastern parts of the area are associated with major tectonic lineaments and active NE trending faults (PERISSORATIS et al., 1995). All volcanic products, from basalt to rhyolite, belong to the calc-alkaline series. In the western sector (e.g. Corinth, Aegina, Methana, Poros) the presence of numerous domes and lava flows of andesitic to dacitic composition dominate the volcanic edifice. Pyroclastics are subordinate or missing (DIETRICH et al. 1988, 1994, 1995; MITROPOULOS and TARNEY, 1992). These intermediate rock

[1] Institute of Mineralogy and Geology, Agricultural University of Athens, GR-11855 Athens, Greece. <egartz@auadec.aua.gr>

[2] Institute of Mineralogy and Petrography, ETH Zürich, CH-8092 Zürich, Switzerland. Corresponding author. <wumme@erdw.ethz.ch>

types are probably derived from a water bearing basaltic parent by magma crystal-liquid fractionation involving mainly olivine, clinopyroxene, plagioclase, amphibole, biotite and Ti-magnetite, as well as by magma mixing and mingling processes in deep crustal magma reservoirs (DIETRICH et al., 1988). Large central volcanoes with summit calderas and hydrothermal systems (FYTIKAS et al., 1984 and 1986) dominate the central and eastern sectors of the arc (e.g. Milos, Santorini, Kos, Nisyros). Pyroclastic rocks of rhyodacitic to rhyolitic composition are predominant. Water-

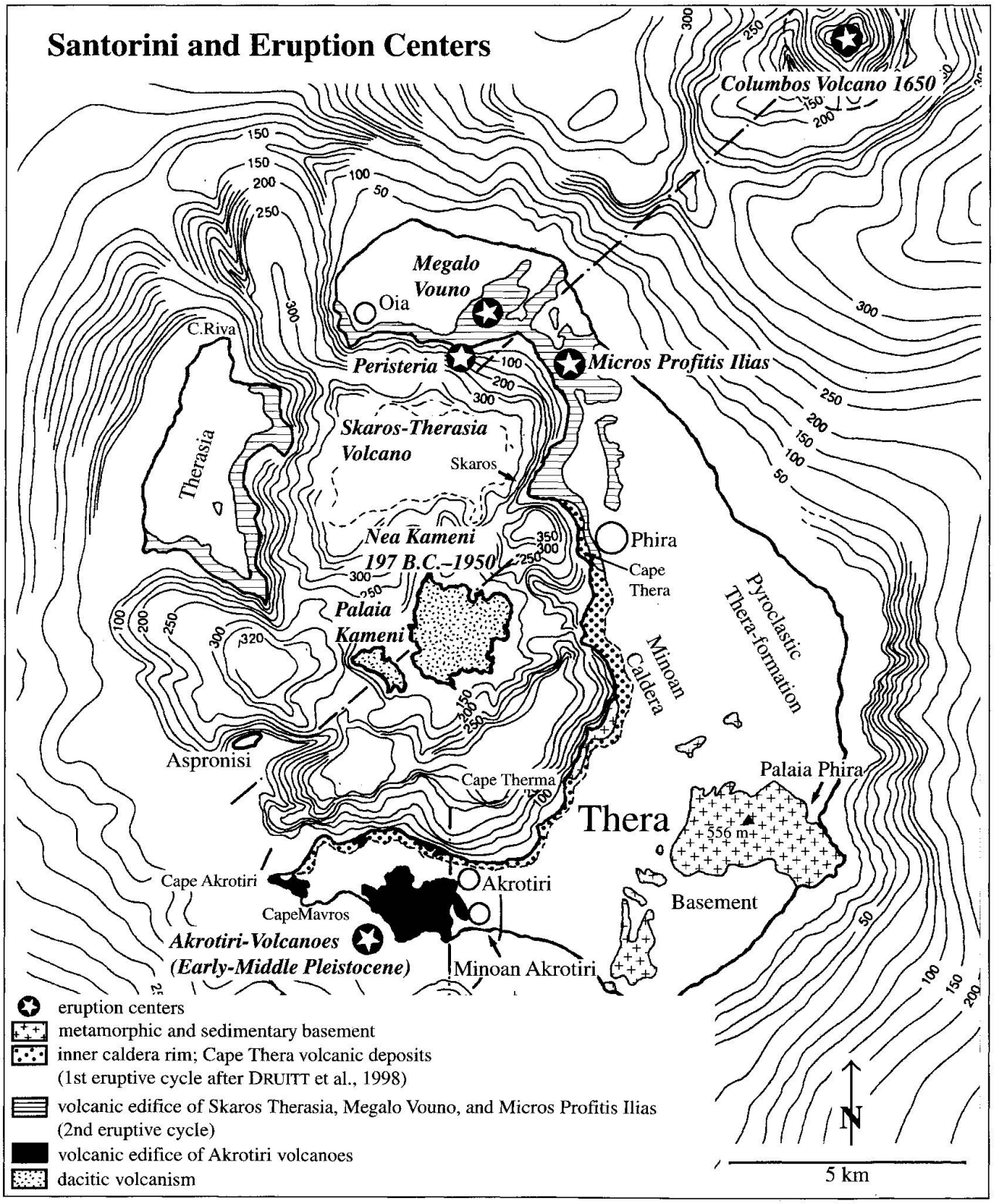

Fig. 1 Santorini islands and eruption centres. Bathymetry after PERISSORATIS et al., 1995.

bearing minerals are subordinate or absent. This indicates relatively large shallow crustal magma chambers, which allowed further crystal fractionation and crustal contamination, finally leading to highly explosive activity and Plinian eruptions.

Magmatic activity and the depth of the magma reservoirs in the different sectors of the Aegean volcanic arc seem to be related to the complexity of the lithospheric stress field (PAPAZACHOS et al., 1992; PAPAZACHOS and PANAGIOTOPOULOS, 1993). The western sector of the arc seems to have experienced a lesser extensional regime than the central and eastern sectors. Upwelling of the asthenosphere, partial melting, uprise of primitive basaltic melts and the generation of shallow magma chambers beneath Milos, Santorini and Nisyros is favoured today by a pronounced tensional regime.

In contrast, the Akrotiri volcanic complex, the oldest volcanic edifice of the Santorini islands, is very similar to the volcanic edifice in the western sector (DAVIS et al., 1996). A major shift of the tectonic regime may have occurred a few hundred thousands years ago, leading to the large pyroclastic eruptions of the "Main Volcanic Series" and formation of large calderas (DRUITT, 1996; DRUITT et al., 1998; DRUITT and FRANCAVIGLIA, 1992), typical for the central and eastern sectors.

However, from 1649 to 1650 a new volcano (Columbos, Fig. 1) erupted only a few kilometres north-east of Santorini, producing rhyodacitic pumice and andesitic lavas, which contain magmatic inclusions and amphibole as major mafic phase, again very similar to those in the Akrotiri volcanic complex (VOUGIOUKALAKIS et al., 1996).

The objectives of this study are to describe the bulk-rock composition of the Akrotiri lavas as well as the mineral chemistry of phenocrysts, xenocrysts, groundmass minerals, and glass compositions in coexisting inclusions and host lava pairs in order to discuss the following processes:

1) bulk-rock crystal fractionation;

2) magma mixing or mingling between rhyodacite and basaltic to andesitic melts, forming magmatic inclusions as well as the compositionally heterogeneous andesites and dacites;

3) magma mixing between andesitic and basaltic melts; and to construct a model of a stratified magma chamber which may account for the above processes during periods of replenishment.

Amphibole/plagioclase fractional crystallisation, magma mixing and mingling are discussed to explain the difference of the magmatic processes and eruption modes between the oldest and younger volcanic cycles of the Santorini islands. A better understanding of the eruption behaviour of the Aegean arc volcanism could be helpful to predict volcanic eruptions.

2. Geological setting of Akrotiri Volcanic Complex

The Akrotiri Volcanic Complex (AVC) forms the southern part of the Santorini islands (Fig. 1 and Tab. 1). It is bordered from all other volcanic complexes as well as from the metamorphic crystalline and sedimentary Mesozoic basement rocks by a depression along a N–S trending fault and graben zone. The Akrotiri complex is composed of the oldest volcanic rocks on the islands of Santorini with ages probably ranging from 1.6 to 0.5 Ma (FOUQUÉ, 1879; FYTIKAS et al., 1976; SEWARD et al., 1980; FYTIKAS et al., 1984; SEIDENKRANTZ and FRIEDRICH, 1992).

A reconstruction of the Plio- to Pleistocene volcanic history of the Akrotiri Volcanic Complex (Fig. 2) is very difficult for the following reasons:

– The younger pyroclastic deposits (< 350'000 a) cover large parts of the entire area: e.g. the Cape Therma eruptions; the lower, middle and upper pumice; the upper scoriae; the Cape Riva deposits and finally, the Minoan pumice. These pyroclastic rocks are not shown on figure 2. Only the actually outcropping volcanics of the AVC are drawn.

– The northern parts of the AVC have been destroyed during the formation of the large Santorini calderas (DRUITT, 1985, 1996; DRUITT et al., 1998; DRUITT and FRANCAVIGLIA, 1992).

– The southern and southwestern parts of the AVC are broken off, now forming the sea floor. Their volumes can only be estimated considering the sea floor morphology and lithology (PERISSORATIS et al., 1995).

– Weathering and erosion have drastically affected the original volcanic morphology.

However, a few eruption centers of the Akrotiri volcanic complex are evident (Fig. 2):

1) Rhyodacitic eruption centers (fissures) at the Castle within the village of Akrotiri as well as at Cape Akrotiri.

2) Andesitic to dacitic plugs and fissures are present at Cape Mavros and at Cape Vounia.

3) Basaltic to andesitic fissure eruptions and cinder cones aligned along N–S trending faults at Cape Kokkinopetra, Cape Balos and Cape Mavrorachidi.

4) From morphology along the southern coast and cliffs of the Akrotiri peninsula, and from bathymetry, a large eruption centre can be inferred southwest of Cape Vounia (Fig. 1).

Shallow marine basaltic to rhyolitic volcanism at Santorini began about 1.6 Ma ago and contin-

Tab. 1 Volcanological evolution of the Akrotiri Volcanic Complex (AVC).

< 200'000 a	Thera Volcanic Complex	
360–300'000 a	Cape Therma pumice	
300'000 a	Erosional surface ? time interval	
VOLCANIC CENTRES	**N: Cape Akrotiri/Loumaravi** **S: Cape Mavros/Arkhangelos**	**Cape Balos/Kokkinopetra** **Cape Mavrorachidi**
? 350'000		Basaltic andesite (high-Mg) Cinder cones, dykes, lava
	Andesites and dacites Domes, flows (submarine)	Basalts (IAT, + pyroxene) Cinder cones, dykes, lava
	Erosional surface ? time interval	
? 600'000 a	Andesites (+ amphibole relics) Cinder cones, dykes, lava Dacitic domes, flows (submarine)	
? 1 Ma	Rhyodacites (+ amphibole) Partly submarine pyroclastics tuffs, tuffites, pumice	Rhyodacites (+ amphibole)
? 1.6 Ma	Minor submarine Basalts to andesites (+ amphibole)	(Metamorphic basement)
? > 2 Ma	Pliocene shallow marine sediments No volcanoclastic detritus!	

ued until at least 580'000 a (DRUITT, 1996). The products are hornblende bearing rhyodacitic lavas and tuffs, which form the hills of the Akrotiri peninsula. Abundant amphibole distinguishes the Akrotiri volcanic rocks from the younger Santorini volcanics, which generally lack amphibole.

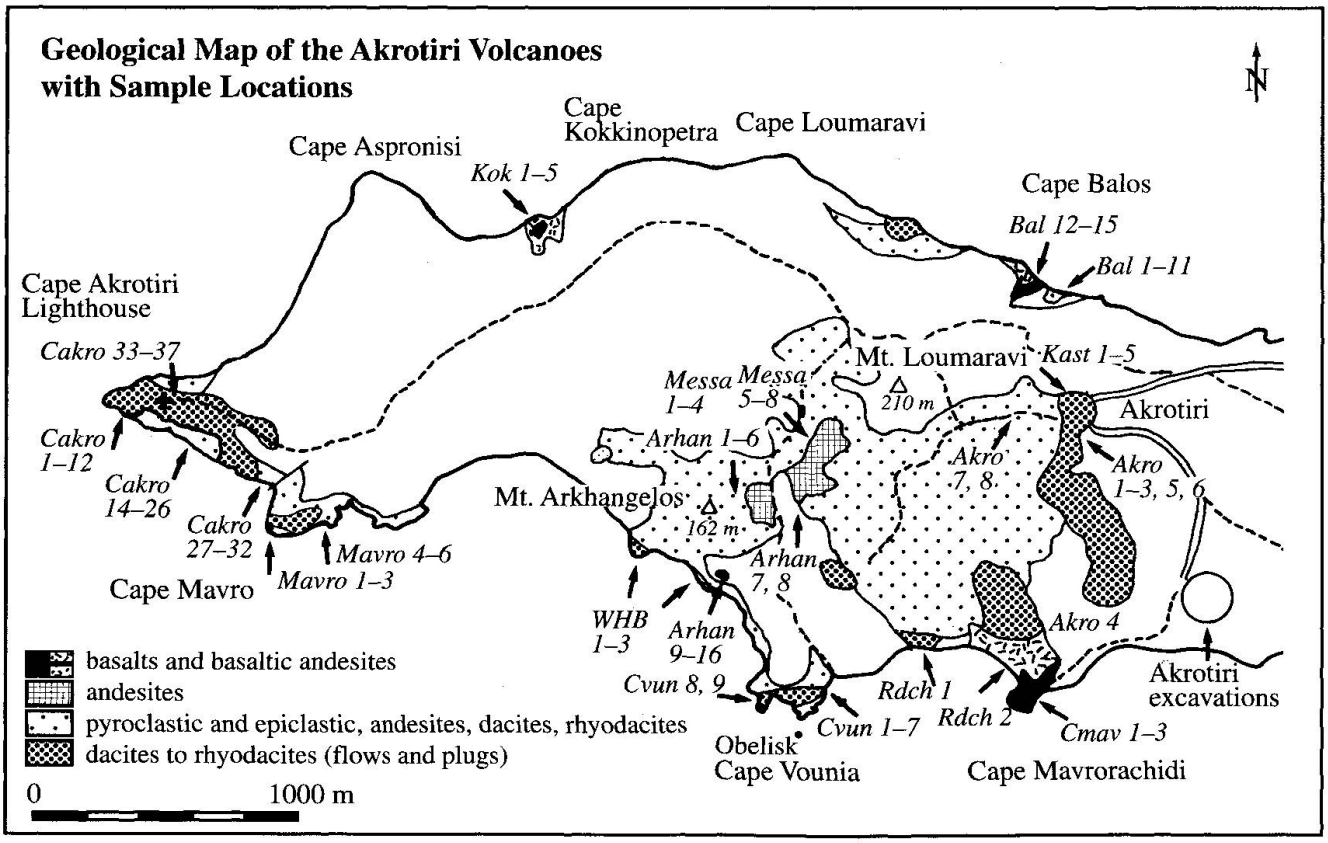

Fig. 2 Geological map of the Akrotiri volcanoes with sample locations; geology in parts after PICHLER and KUSSMAUL, 1980.

Within the Upper Pliocene sediments from the Arkhangelos hill, approx. 1.6 Ma, according to Foraminifera ages (SEIDENKRANTZ and FRIEDRICH, 1992), basaltic and andesitic detritus occurs, partly as fragments of pillow lavas and hyaloclastites. Amphibole appears as a very diagnostic volcanic mineral in the tuffaceous sediments (Fig. 3).

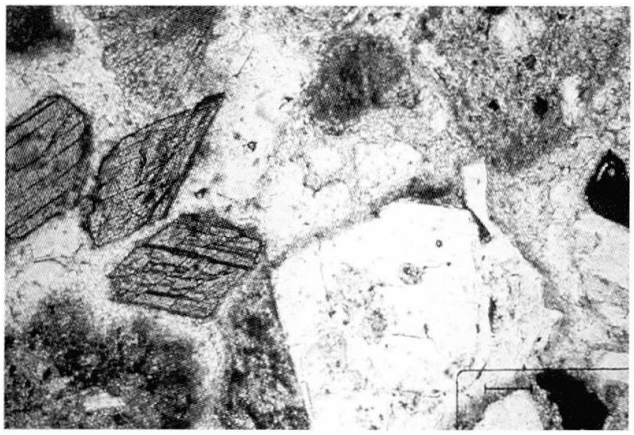

Fig. 3 Green and brown amphiboles in shallow water sandy marls (Pleistocene age) from Mt. Arkhangelos base; figure size: 2.6 mm across.

Prolonged eruption on the sea floor generated a rhyodacitic complex with an original basal diameter exceeding 4 km and a height exceeding 200 m (Fig. 2). In the Loumaravi-Arkhangelos area, submarine domes, pillow lavas dominate the volcanic successions. Hyaloclastite aprons intercalate with submarine vitric tuffs, pumice breccias, and epiclastic flows. At higher elevations, lavas may have erupted subaerially. The occurrence of submarine vitric tuffs, foraminiferous- or sponge-bearing marine sediments, and (at Cape Mavros) hyaloclastite up to heights of 100 m or more above present day sea level implies considerable post-formational volcano-tectonic uplift of these early centers.

The initial volcanic phase was followed by larger eruptions of rhyodacitic to dacitic pyroclastics (tuffs, pumice, and in a few places ignimbrite) and lavas from vents close to Paleokastro (village of Akrotiri) and in the vicinity of Cape Akrotiri (Fig. 2).

The area between Mt. Loumaravi, Mt. Arkhangelos, Cape Vounia and Cape Mavrorachidi is mainly covered with the silicic lavas and pyroclastics, in parts heavily weathered, hydrothermally altered and eroded. Within the southwestern slopes of Mt. Loumaravi and the N–S depression east and southeast of Mt. Arkhangelos, numerous andesitic dikes crosscut the older silicic volcanics. These dikes are also heavily weathered and altered. They exhibit mainly porphyric textures. The appearance of black opacitic amphibole and the high abundance of quartz ocelli (see chapter 3) are very significant.

Similar andesites and andesitic dacites are also found as components within the pumice-rich epiclastic rocks (in parts lahars), which overlay a peneplained yellowish beach conglomerate underneath the lighthouse (Faros) at Cape Akrotiri, approximately 80 m above the present day sea level. The latter feature indicates a large time interval of intensive erosion, probably coupled with uplift.

The andesitic to dacitic domes, sills, flows and pyroclastics of Cape Mavros and Cape Vounia seem to belong to a younger volcanic generation. The dacites show partly intrusive contacts as well as lavas, which reached the submarine environment generating pillows and hyaloclastic breccias.

The youngest volcanic phase in the Akrotiri volcanic complex is represented by basaltic to andesitic extrusions (dikes and cinder cones) at Cape Balos, Cape Kokkinopetra and Cape Mavrorachidi. The latter one seems to be connected with the Cape Balos eruptive centre along an N–S striking fault.

At broadly the same time that the Peristeria stratocone (DRUITT, 1996) was active in northern Santorini (Fig. 1), "strombolian eruptions" in the south formed cinder and spatter cones at Capes Balos, Kokkinopetra, and Mavrorachidi. These cones may have originated from mafic monogenetic vents on the southern flank of the Peristeria edifice. All three cones overlie tuffs and lavas of the early rhyodacitic centers, but underlie the pyroclastic deposits of Cape Therma. The latter relation can clearly be seen at Cape Balos (Fig. 2).

3. Petrography

3.1. LAVAS AND PYROCLASTICS

Table 2 summarises the petrographic and mineralogical characteristics of the Akrotiri lavas in stratigraphic order from bottom (oldest lavas) to top (youngest lavas). The localities of the analysed rock samples as well as their bulk chemical compositions are shown on figure 2 and given in the Appendix.

Basalts and basaltic andesites are massive to slightly vesicular porphyritic rocks. Macrophenocrysts are olivine, plagioclase and subordinate augite in an intersertal to intergranular, partly fluidal groundmass of plagioclase laths, granular pyroxenes, olivine, Ti-magnetite and interstitial glass.

Tab. 2 Summary of petrographic and mineralogical characteristics of the Akrotiri lavas in stratigraphic order (from bottom to top). P = phenocryst; M = microphenocryst; X = xenocryst; I = inclusions in phenocryst phases; ( ) = rare occurrences.

	Plag	Cpx	Opx	Amph	Fe–Ti Oxides	Ol	Ap	Zr	Cr-spinel
Basalts	P, M, X	P, M	M	–	P, M	P, M	?	?	I
Basaltic andesite	P, M, X	P, M	P, M, X	(X ?)	P, M	P, M	I	?	I
Andesitic Dacite	P, M, X	P, M	P, M	(X ?)	P, M	X	I	(M, I)	–
				2nd cycle					
Andesite	P, M, X	P, M	(M) X	(P, X)	P, M	P, M	I	(I)	I
Dacite	P, M, X	P, M	P, M	P, M, X	P, M	–	M	(M, I)	–
Rhyolite to rhyodacite	P, M, X	P, M	P, M	P, M, X	P, M	–	M	(M, I)	–
Submarine basalts to andesite	P, M	P, M	–	P, M	M	?	?	?	?
				1st cycle					

Basalts of Cape Balos occur as pyroclastics (scoria) at the base of the Balos plug and as massive lavas or sills. They are slightly vesicular and weakly porphyritic. Macrophenocrysts are olivine, plagioclase and subordinate augite in an intersertal to intergranular, partly fluidal groundmass of plagioclase laths, granular pyroxenes, olivine, Ti-magnetite and interstitial glass.

The *basaltic andesites* can be distinguished from the basalts by the presence of clinopyroxene and plagioclase xenocrysts with inverse compositional zoning.

The *andesites* are strongly porphyritic with normally zoned plagioclase macrophenocrysts and subordinate augite and hypersthene. Olivine is altered. The pilotaxitic matrix consists of andesine laths, prismatic pyroxenes, magnetite and interstitial altered glass.

Andesitic dacites and dacites: According to the bulk chemical classification (see chapter 5; e.g. the differentiation index D.I) these volcanic rocks should be named andesites. However, the partially high abundance (e.g. 30–50 vol.%) of basic magmatic inclusions and xenocrysts (e.g. plagioclase An_{86-75} and amphibole) as well as the rhyodacitic to rhyolitic groundmass glass justifies the terminology andesitic dacite or dacite.

These rocks often contain a glassy, flow banded, hyalopilitic groundmass with large amounts of isolated plagioclase (often rich in melt inclusions and sieve textures) and augite phenocrysts, glomeroporphyritic clots of euhedral, weakly zoned plagioclase (An_{64-50}), orthopyroxene (En_{71-64}), augite, and magnetite, and glass. Andesine laths, acicular pyroxenes and apatite occur as microphenocrysts. In the andesitic dacites and dacites of Cape Mavros and Cape Vounia the matrix glass is in parts fairly fresh, amphibole is missing as phenocrysts as well as xenocrysts.

The *rhyodacites* are generally glassy and flow banded rocks, often with a felsitic or vitrophyric matrix. Plagioclase (phenocrysts An_{55-40}), amphiboles (cores: tschermakitic rimmed by magnesio hornblende) and orthopyroxene (En_{69-65}; in rhyolitic components En_{45-42}) occur as macrophenocrysts, magnetite and ilmenite as microphenocrysts. The glass has rhyodacitic to rhyolitic composition. Figure 4 shows a typical rhyodacite as a microscopic drawing by FOUQUÉ (1879). Empty spaces in the rhyolitic groundmass glass are partially filled with calcite and zeolites.

Flows of entirely rhyolitic composition are missing.

3.2. AMPHIBOLE – PLAGIOCLASE INCLUSIONS

One of the most striking features of the rhyodacitic and dacitic lavas is the irregular distribution of dark mafic xenolithic inclusions, mainly consisting of hastingsitic amphibole and plagioclase in a porous glassy groundmass. These clots and spheres vary in size from a few millimetres to approximately 20 centimetres in diameter; the average dimension is 5 to 10 cm. The flow banding of the rhyodacitic lava aligns with the orientation of their geometry. Blocky and fragmented inclusions with subangular surfaces are very subordinate.

The distribution of the inclusions in the lavas is highly variable. They are more abundant in the lower rhyodacites and dacites of the first volcanic cycle. An estimation of their volume percentage is very difficult. There are portions of the flows with 10 to 20 vol.% of inclusions, but in general the variation ranges between 1 and 3 vol.%. In the dacites and andesites of the second volcanic phase the inclusions decrease to less than 1 vol.%.

In general, the inclusions in the andesitic dacites and dacites of the first volcanic phase show distinct differences in textures and composition to those from the basaltic andesites and andesites of the second cycle, and they are almost absent in the basaltic andesites of Cape Mavrorachidi.

In the dacites, several types of inclusions can be distinguished:

Type A: Basaltic inclusions with typical porphyritic and intersertal textures and olivine, clinopyroxene (rimmed by amphibole), plagioclase in a basaltic groundmass glass. They are very rare and rather small in size (0.1 to 2 cm in diameter; e.g. sample Cakro 5, bulk chemical composition in table A3, Appendix).

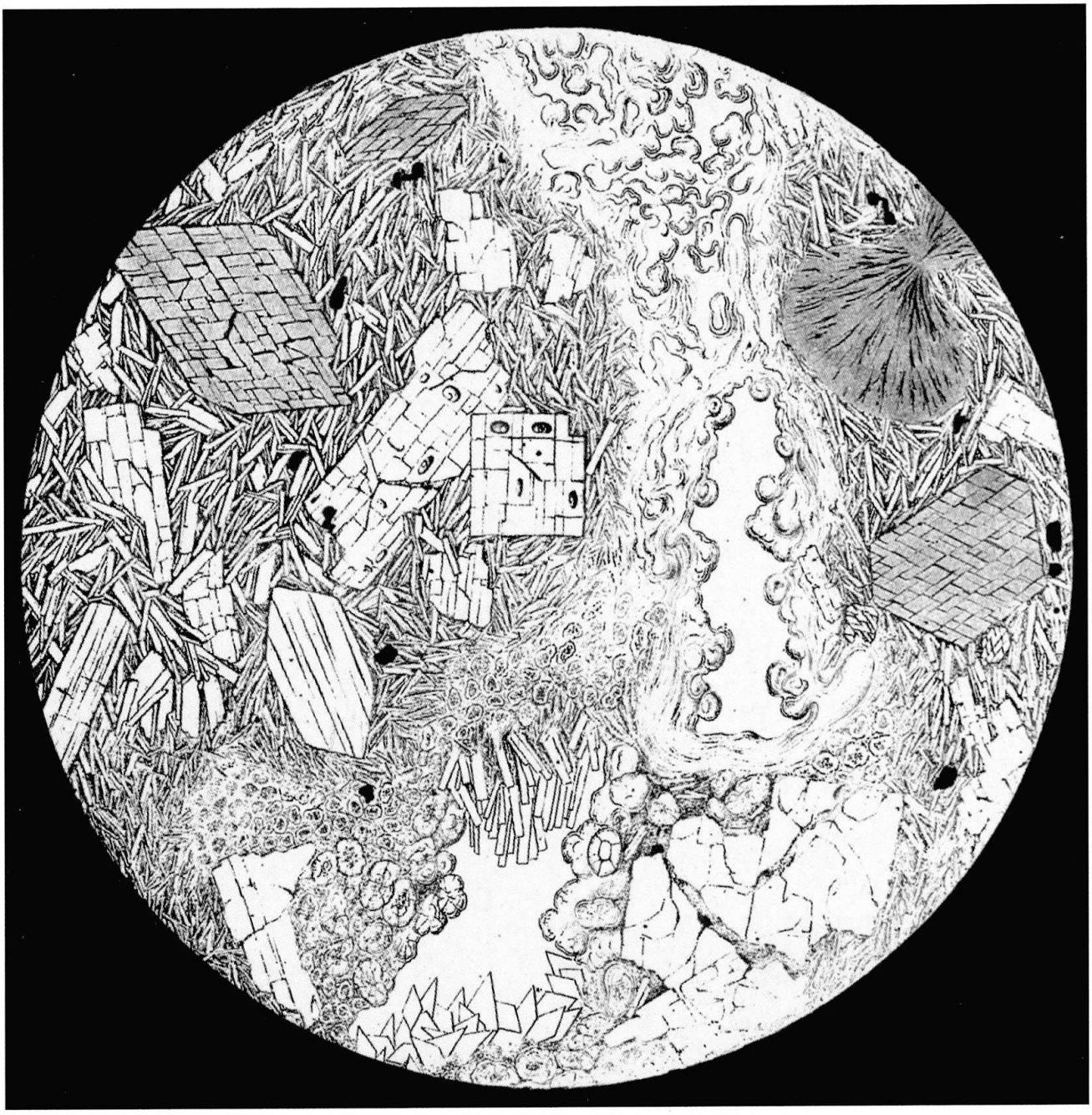

Fig. 4 Magnesio-hornblende, plagioclase and orthopyroxene in rhyodacite (Cape Akrotiri); rhyolitic groundmass glass partly filled with carbonate and zeolites. Figure size 3 mm across. Drawing from FOUQUÉ (1879).

Type B: Cumulates are very sparse. These rocks are rather small in size, generally not exceeding 5 cm in diameter.

Type C: Pseudocumulates with partly resorbed (remolten) cumulate minerals such as Mg-rich hastingsitic amphibole and anorthite-rich plagioclase in an interstitial glass rich in silica, K, Rb, Sr, Ba. They are also very rare.

Types D, E and F: Coarse-grained acicular inclusions (Fig. 7), mainly made up of amphibole and plagioclase in a glassy (chemical composition in Tab. A3, Appendix) but highly porous matrix, are very abundant. The composition varies from basaltic to andesitic.

Type D inclusions are by far the most common ones. They also contain fragments or inclusions of type B cumulates and type C pseudocumulates. The rounded and elliptical shapes may be caused by rapid undercooling during injection of hot basaltic and andesitic melts into a magma reservoir filled with cooler dacitic to rhyodacitic melt (EICHELBERGER, 1980; BACON, 1986; DIETRICH et al., 1988; DIETRICH, 1989; FEELEY and DUNGAN, 1996). Therefore, the xenolithic inclusions can also be regarded as important witnesses with respect to magmatic processes in deep-seated reservoirs, and in particular to the generation of highly differentiated basalts and andesites.

4. Mineralogy

4.1. MINERAL CHEMISTRY

The mineralogical characteristics of the Akrotiri lavas are summarised in table 2; the mineralogical compositions of the analysed rock-samples are given in table 3.

Special emphasis has been given to the mineral chemistry of clinopyroxenes, amphiboles, Fe–Ti oxides and Cr-spinels, and of groundmass glass. The selected microprobe mineral analyses are listed in tables 4 to 7.

The general crystallisation sequence in the early Akrotiri lavas appears to be olivine + Cr-spinel, plagioclase, clinopyroxene, Mg-hastingsitic amphibole, Ti-magnetite, orthopyroxene, apatite and zircon. In the late Akrotiri lavas it is plagioclase, clinopyroxene, tschermakitic hornblende, magnesio hornblende, magnetite, ilmenite, orthopyroxene, apatite and zircon. Alkali feldspar and quartz occur sporadically in the rhyolitic pumice.

Plagioclase is present in all rocks as the most abundant phenocryst phase and forms euhedral crystals up to a few millimetres in size. The compositions are given in terms of anorthite content in the rock description and range from An_{85} in the basalts to An_{29} in the rhyodacites. The phenocryst

Tab. 3 Minerals compositions within the Akrotiri volcanics (Mg-Hst = Magnesio-hastingsite; Tsch = Tschermakite; Mg-Ho = Magnesio-hornblende; r = rim, inter = intermediate, c = core; grd = groundmass; n.a. = not analysed).

	Cape Balos high-alumina olivine basalt	*Cape Mavrorachidi* high-Mg basaltic andesite	*Cape Vounia* andesites	*Cape Mavros* andesites to dacites	*Akrotiri* rhyodacite	*Akrotiri* rhyolites	*Akrotiri* basic inclusions in rhyodacite
Plagioclase macro-phenocryst. micro-phenocryst.	An_{85-74} An_{69-63}	$An_{60-52(c)}$ $An_{74-68(r)}$ An_{73-70}	$An_{75-64(c)}$ $An_{49-37(r)}$ An_{40-37}	An_{49-45} An_{65-49}	$An_{(65)55-49}$ An_{45-40} and An_{31-29}	An_{51-45} and An_{54-36} An_{31-29}	$An_{86-81(c)}$ $An_{77-60(inter)}$ $An_{46-60(r)}$
Olivine	Fo_{85-82}	Fo_{84-77}	Fo_{80-75}	–	–	–	-
Clino-pyroxene	$xMg,(Fe_{tot})$ = 0.80–0.68	$xMg,(Fe_{tot})$ = 0.75–0.69(c) $xMg,(Fe_{tot})$ = 0.83–0.84(r)	$xMg,(Fe_{tot})$ = 0.78–0.74	$xMg,(Fe_{tot})$ = 0.78–0.74	$xMg,(Fe_{tot})$ = 0.78–0.74		very rare (e.g. Cakro5, $xMg,(Fe_{tot})$ = 0.80–0.75)
Ortho-pyroxene	En_{72-69}	En_{67-66}	En_{71-64}	En_{69-66}	En_{68-64} and En_{47}	En_{45-42}	En_{58-55}
Amphibole	–	relicts	relicts	Tsch	Tsch(c) Mg-Ho(r)	Tsch(c) Mg-Ho(r)	Mg–Hst Tsch
Cr-spinel	in olivine	(in Cpx or Ol)	–	–	–	–	–
Fe–Ti oxides	Ti-magnetite	(in Cpx or Ol) grd-ilmenite	Ti-magnetite grd-ilmenite	Ti-magnetite and ilmenite	Ti-magnetite and ilmenite	Ti-magnetite and ilmenite	Ti-magnetite
Xenocrysts Plag / Opx	n.a. Plag, Opx	An_{88}, Fo_{90}, Cpx, xMg = .88	An_{87-75}	An_{85-82}	An_{82-78} and An_{93-92}	An_{85-82}, En_{69-66}	An_{85-82}

Tab. 4 (A) Selected clinopyroxene compositions in Cape Balos basalt (Bal 8 and 15) and in Cape Mavros andesite (Mavro 2). (B) Selected clinopyroxene compositions in high-Mg basaltic andesite Cape Mavrorachidi (Cmav 2). (C) Selected clinopyroxene compositions in andesite Cape Vounia (Cvun 7).

(A)	C. Balos basalt phenocrysts			C. Mavros	macro-phenocrysts			
wt%				core	rim	rim	core	rim
	178	185	186	230	229	228	241	232
SiO_2	50.65	50.16	49.47	51.72	51.46	49.52	52.17	49.74
TiO_2	0.84	0.91	1.18	0.44	0.73	0.94	0.49	0.86
Al_2O_3	3.38	3.88	4.97	1.65	2.46	3.86	1.77	3.60
Cr_2O_3	0.40	0.52	0.80	0.01	0.03	0.00	0.00	0.06
Fe_2O_3	1.03	1.62	0.26	3.24	2.63	3.52	2.79	3.69
FeO	7.13	6.67	7.27	6.44	7.06	6.28	5.75	5.38
MnO	0.16	0.25	0.16	0.45	0.44	0.29	0.43	0.31
NiO	0.08	0.05	0.03	0.03	0.00	0.00	0.00	0.01
MgO	15.86	16.25	14.74	16.01	15.14	14.70	16.31	14.74
CaO	20.01	19.39	20.66	19.78	20.34	20.14	20.44	20.88
Na_2O	0.00	0.00	0.00	0.31	0.35	0.32	0.29	0.32
K_2O	0.02	0.01	0.00	0.01	0.01	0.00	0.01	0.01
Total	99.55	99.71	99.54	100.09	100.64	99.57	100.44	99.61
xMg(Fe_{tot})	0.80	0.78	0.78	0.75	0.74	0.74	0.78	0.75
Wo	0.351	0.328	0.350	0.363	0.364	0.342	0.371	0.357
En	0.440	0.450	0.410	0.443	0.417	0.409	0.447	0.410
Fs	0.111	0.103	0.113	0.100	0.109	0.098	0.088	0.084

(B)	macro-phenocrysts						micro-phenocrysts	
wt%	core	rim	core	rim	core	rim		
	141	142	104	106	137	147	82	83
SiO_2	51.31	51.31	51.36	51.82	51.40	50.64	51.25	51.93
TiO_2	0.69	0.53	0.69	0.42	0.80	0.78	0.40	0.33
Al_2O_3	2.10	3.98	2.39	3.70	1.88	3.92	3.96	2.90
Cr_2O_3	0.06	0.58	0.17	0.87	0.04	0.37	0.76	0.42
Fe_2O_3	2.29	2.11	2.85	2.95	2.43	3.72	2.58	2.70
FeO	9.73	4.38	8.15	2.80	10.05	4.73	3.31	4.17
MnO	0.40	0.11	0.27	0.12	0.45	0.26	0.12	0.17
NiO	0.00	0.00	0.00	0.00	0.03	0.00	0.08	0.05
MgO	14.51	16.91	15.67	17.23	14.89	16.15	16.89	17.66
CaO	18.95	20.31	18.81	21.32	18.20	20.36	20.56	19.91
Na_2O	0.36	0.25	0.34	0.29	0.38	0.30	0.36	0.21
K_2O	0.01	0.01	0.00	0.02	0.01	0.00	0.01	0.03
Total	100.41	100.49	100.71	101.53	100.56	101.23	100.27	100.47
xMg(Fe_{tot})	0.69	0.83	0.72	0.85	0.75	0.78	0.84	0.83
Wo	0.346	0.340	0.332	0.352	0.333	0.333	0.343	0.340
En	0.404	0.460	0.432	0.463	0.414	0.439	0.461	0.481
Fs	0.152	0.067	0.126	0.071	0.157	0.072	0.050	0.064

(C)	Cvun 7/Andesite lava basaltic inclusion			phenocrysts		plag/cpx/Ti-mgt cluster		micro-phenocryst
wt%	158	159	160	113	123	173	175	129
SiO_2	48.78	46.51	50.76	50.21	50.21	52.02	50.81	51.39
TiO_2	1.49	1.90	0.63	0.95	0.72	0.51	0.82	0.51
Al_2O_3	5.70	6.84	2.52	3.33	2.89	1.99	2.53	1.81
Cr_2O_3	0.04	0.02	0.04	0.00	0.10	0.01	0.02	0.04
Fe_2O_3	3.66	3.88	2.27	3.22	3.79	1.58	2.52	2.60
FeO	6.20	4.84	7.28	7.57	4.95	7.27	6.44	6.68
MnO	0.23	0.18	0.25	0.42	0.38	0.44	0.40	0.51
NiO	0.02	0.00	0.00	0.00	0.06	0.01	0.00	0.02
MgO	13.93	13.17	15.67	15.13	14.98	15.42	14.86	15.11
CaO	20.92	21.45	19.36	19.05	21.08	20.31	20.76	20.50
Na_2O	0.34	0.29	0.21	0.32	0.33	0.31	0.34	0.32
K_2O	0.00	0.00	0.00	0.01	0.01	0.00	0.01	0.00
Total	101.31	99.08	98.99	100.21	99.55	99.85	99.50	99.49
X_{Mg}(Fe_{tot})	0.72	0.74	0.75	0.72	0.76	0.76	0.75	0.75
Wo	0.331	0.334	0.348	0.326	0.369	0.377	0.376	0.378
En	0.383	0.369	0.438	0.419	0.418	0.427	0.414	0.421
Fs	0.096	0.076	0.114	0.118	0.077	0.113	0.101	0.104

compositions in the basic inclusions range from An_{86} in the cores to An_{44} in the rims. The phenocrysts in the basaltic andesites show reversed, in the andesites normal (Fig. 5), but complex compositional zoning. Sieve-textures and resorption phenomena are also common in the latter. Plagioclase xenocrysts are very frequent in the dacites, rhyodacites and rhyolites. They often exhibit rounded, dusty cores with bytownitic compositions An_{93-75} overgrown by optically clear and distinctive rims of intermediate compositions. Microphenocryst laths range in composition from An_{74-63} in the basalts and basaltic andesites, An_{65-37} in andesites, An_{45-29} in dacites, rhyodacites and rhyolites (Fig. 5).

Alkali feldspar with 8–12 mol% orthoclase as well as quartz occur in small quantities in the rhyolites.

Olivine phenocrysts and microphenocrysts are common in the Akrotiri basalts and basaltic andesites. The crystals are relatively small (< 1 mm) and exhibit euhedral, anhedral and quenched shapes. Their compositions range from Fo_{85} to Fo_{82} in the basalts, Fo_{84} to Fo_{87} basaltic andesites and Fo_{80} to Fo_{75} in the andesites. The Ni- and Mn-contents vary proportionally to the iron enrichment in the olivine (e.g. in the basalts: NiO = 0.22 to 0.14 wt%, MnO = 0.21 to 0.25 wt%).

Clinopyroxene (Tab. 4) is a common phenocryst phase in all rocks except in the rhyolitic pumice and rhyolitic components in the lowermost Akrotiri pyroclastics. The xMg values range from 0.80 to 0.68 in the basalts and 0.76–0.72 in the andesites,

dacites and rhyodacites. The general decrease of MnO in the rhyodacites and rhyolites is noteworthy. The clinopyroxenes in the basaltic andesites exhibit reverse zoning (Fig. 6, xMg = 0.75 to 0.69 in the cores; xMg = 0.83 to 0.84 in the rims) which is thought to indicate magma mixing. This is clearly expressed in their Cr- and Mn-contents: the cores are low in Cr_2O_3 up to 0.2 wt% but high in MnO up to 0.45 wt%, whereas the rims are high in Cr_2O_3 up to 0.9 wt% and low in MnO between 0.11 and 0.17wt%.

Orthopyroxene is also a common phenocryst phase in all rocks. It occurs subordinate as resorbed xenocrysts rimmed by clinopyroxene in basaltic andesites and andesites. All crystals show a restricted compositional range and only weak zonation: En_{72-69} in the basalts, En_{69-66} in the andesites, En_{68-64} in the dacite to rhyodacites, and En_{45-42} in the rhyolites.

Fe–Ti oxides (Tab. 5) are common as euhedral to anhedral phenocrysts, as inclusions in other phenocryst phases, and as reaction products within and between amphiboles and clinopyroxenes (Fig. 8 and 9). Ti-magnetite occurs in basalts and in basaltic andesites, but is rather rare. It only occurs within larger clinopyroxene xenocrysts (Tab. 5C). Instead, ilmenite is present in the ground-

Tab. 5 (A, B) Selected representative analyses of Fe–Ti oxides.

(A)	Cakro 19 Rhyolite	Bal 3 Rhyodacite	Rdch 1/Rhyodacite					
wt%	310	22	127	157	204	10	158	156
SiO_2	0.08	0.02	0.00	0.00	0.00	0.06	0.00	0.00
TiO_2	7.86	7.00	8.17	39.81	6.81	6.89	39.41	40.22
Al_2O_3	1.36	1.97	1.98	0.12	1.58	2.01	0.12	0.12
Cr_2O_3	0.09	0.07	0.26	0.23	0.26	0.07	0.23	0.20
Fe_2O_3	49.80	53.77	52.62	27.38	55.00	54.20	27.50	27.18
FeO	36.65	34.22	35.44	31.08	34.22	34.77	31.16	31.31
MnO	0.36	0.74	0.76	0.83	0.82	0.70	0.75	0.79
NiO	0.03	0.06	0.22	0.19	0.24	0.01	0.19	0.22
MgO	0.34	1.64	1.81	1.93	1.46	1.55	1.69	2.00
CaO	0.01	0.04	0.04	0.07	0.09	0.07	0.09	0.08
K_2O	0.00	0.01	0.05	0.05	0.06	0.00	0.07	0.06
Total	96.58	99.54	101.35	101.69	100.53	100.33	101.19	102.19
Ulvöspinel	0.32	0.20	0.22		0.19	0.19		
Ilmenite				0.65			0.66	0.65

(B)	Cakro 12/Basic Inclusion in Cakro 1				Cakro 11/Basic Inclusion in Cakro 1			
wt%	57	59	62	61	65	66	67	70
SiO_2	0.00	0.00	0.02	0.52	0.05	0.05	0.02	0.00
TiO_2	9.60	14.09	8.28	0.17	9.46	7.23	9.63	8.69
Al_2O_3	1.79	2.46	2.27	0.00	6.01	4.33	2.31	6.87
Cr_2O_3	0.21	0.23	0.19	0.19	0.21	0.22	0.23	0.22
Fe_2O_3	47.92	36.89	47.86	65.25	42.81	49.08	46.97	44.49
FeO	37.51	41.63	36.04	30.01	35.78	34.22	37.14	35.07
MnO	0.65	0.65	0.66	0.12	0.17	0.23	1.08	0.23
NiO	0.21	0.19	0.21	0.24	0.18	0.18	0.19	0.17
MgO	0.42	0.51	0.45	0.17	2.39	1.76	0.90	2.62
CaO	0.10	0.17	0.21	0.09	0.09	0.13	0.07	0.10
K_2O	0.04	0.05	0.05	0.06	0.06	0.11	0.03	0.09
Total	98.02	96.87	96.25	96.80	97.22	97.53	98.59	98.55
Ulvöspinel	0.26	0.41	0.24	0.05	0.26	0.21	0.28	0.24

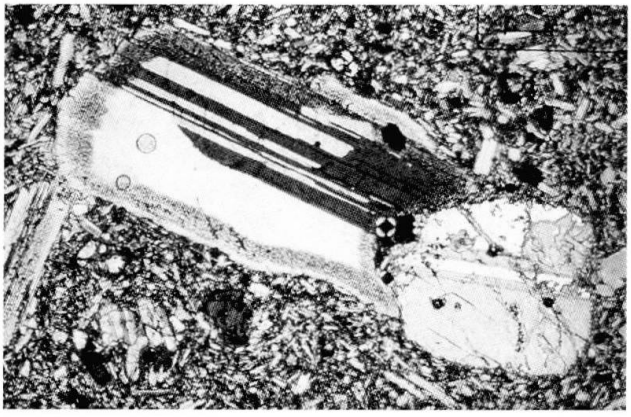

Fig. 5 High-Mg basaltic andesite (Cmav2, Cape Mavrorachidi); figure size: 2.6 mm across. Plagioclase with reverse compositional gap indicating mixing: core (An_{63-52}), transitional dusty zone (An_{67-70}), clear rim (An_{70-75}).

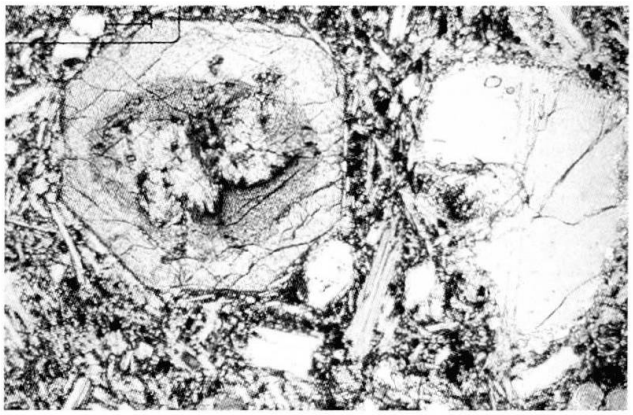

Fig. 6 High-Mg basaltic andesite (Cmav 2, Cape Mavrorachidi); figure size: 2.6 mm across. Clinopyroxene: core xMg(Fe_{tot}) = 0.75–0.69; euhedral rim xMg(Fe_{tot}) = 0.83–0.84 in a basaltic groundmass of plagioclase (An_{73-70}), forsteritic olivine and Fe–Ti oxides. Note that the inner part of the clinopyroxene shows and opaque mixture of fine aggregates that might be interpreted as decomposition products of a former amphibole.

Tab. 5 (cont.) (C) Selected representative analyses of Fe–Ti oxides and Cr-spinels.

(C)	Cmav 2	Cmav 3		Cmav 2/Inclusions in olivine				
	Basaltic andesite			Basaltic andesite				
wt%	ground-mass	Incl. in large cpx	Incl. in plag					
	96	57	78	100	101	62	74	76
SiO_2	0.19	0.44	0.00	0.00	0.00	0.00	0.00	0.00
TiO_2	49.07	2.08	2.02	0.38	0.58	0.38	0.51	0.40
Al_2O_3	0.08	2.59	2.21	15.61	15.84	12.23	17.11	14.19
Cr_2O_3	0.10	1.69	11.48	37.77	40.52	46.32	43.62	41.02
Fe_2O_3	6.22	59.50	49.89	14.62	12.37	11.97	9.76	14.08
FeO	40.90	26.10	28.30	25.29	22.69	22.20	20.31	22.09
MnO	0.43	0.25	0.64	0.00	0.00	0.60	0.47	0.50
NiO	0.00	0.35	0.13	0.06	0.10	0.10	0.05	0.07
MgO	1.38	4.02	2.19	6.03	7.93	7.57	9.58	7.62
CaO	0.17	0.25	0.05	0.01	0.01	0.01	0.01	0.01
Na_2O	0.01	0.00	0.00	0.00	0.00	0.00	0.00	0.02
K_2O	0.10	0.00	0.00	0.00	0.00	0.00	0.00	0.00
Total	98.65	97.28	96.92	99.78	100.03	101.38	101.42	99.99
Hercynite			0.61	0.13	0.09	0.09	0.06	0.07
Chromite			0.02	0.15	0.21	0.23	0.25	0.20
Mg-Chromite			0.15	0.35	0.32	0.36	0.29	0.32
Spinel			0.10	0.06	0.06	0.06	0.05	0.07
Ulvöspinel		0.06						
Ilmenite	0.87							

(C cont.)	Cvun 7/cpx-plag cluster in andesite			Cvun1/cpx-plag cluster in andesite		Mavro 2/ Andesite to Dacite		
wt%	109	177	164	293	274	219	226	258
SiO_2	0.08	0.18	0.18	0.07	0.04	0.25	0.13	0.41
TiO_2	11.30	12.09	12.30	12.51	11.36	15.56	13.26	13.44
Al_2O_3	2.65	3.07	2.90	2.85	2.57	2.13	2.66	2.60
Cr_2O_3	0.10	0.13	0.10	0.15	0.09	0.11	0.13	0.10
Fe_2O_3	45.24	41.51	41.08	41.68	44.58	36.79	40.24	38.42
FeO	37.94	37.28	39.83	38.97	37.43	42.06	40.06	40.23
MnO	0.47	0.44	0.50	0.44	0.57	0.72	0.67	0.57
NiO	0.04	0.00	0.00	0.00	0.00	0.01	0.00	0.08
MgO	2.35	2.78	1.51	2.22	2.43	2.05	1.93	1.75
CaO	0.00	0.04	0.05	0.00	0.02	0.03	0.00	0.05
K_2O	0.02	0.02	0.00	0.01	0.01	0.02	0.01	0.02
Total	100.21	97.54	98.45	0.02	99.08	99.72	99.10	97.68
Ulvöspinel	0.31	0.34	0.32	0.35	0.32	0.43	0.37	0.38

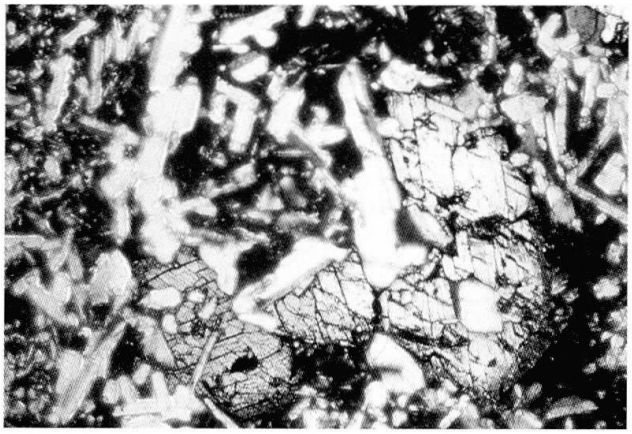

Fig. 7 Large magnesio-hastingsite amphiboles, plagioclase in a porous glass-rich groundmass of rhyolitic composition (black). Coarse grained acicular inclusion (Cakro 11) in rhyodacite (Cape Akrotiri); figure size 5 mm across.

mass. In contrast, Ti-magnetite is always abundant in andesites and dacites and varies in composition from Usp_{43} in the andesites (Tab. 5C) to Usp_{19} in rhyodacites and rhyolites (Tab. 5A). Ilmenite mainly occurs in the evolved rhyodacites to rhyolites. Ti-magnetite is also always present in the gabbroic clinopyroxene-plagioclase clusters as well as in the basic inclusions in the dacitic and rhyodacitic lavas. (Compositional variation: Usp_{41-21} with high Al_2O_3 contents up to 6.9 wt%; Tab. 5B).

Cr-spinel has only been detected as inclusions in olivine and rarely as hercynitic inclusions in anorthitic plagioclase (Tab. 5C).

4.2. AMPHIBOLES AS PHENOCRYSTS AND XENOCRYSTS

Amphiboles are the most common mafic minerals in the volcanic rocks from the Akrotiri volcanoes. They occur as pheno- and xenocrysts in rhyodacitic and dacitic rocks. However, the amphiboles show a large variation in mineral chemistry from Mg-rich hastingsite through evolved hastingsite to hornblende (Tab. 6). Mg-rich hastingsitic amphibole and anorthitic plagioclase are present in various proportions as the two major xenocryst phases in most of the lavas and therefore play a key role with respect to fractional crystallisation processes (DIETRICH et al., 1996).

The amphibole compositions, using the nomenclature of LEAKE (1978), were normalised by assuming (i) fixed $Fe^{3+}/(Fe^{3+} + Fe^{2+})$ ratio of 0.2 and 23 oxygens, and (ii) cations – Ca–Na–K = 13. In the rhyodacites the amphiboles display greenish to light brownish pleochroic colours and ideal euhedral shapes (Fig. 7). They have opacitic reaction rims in a few cases. Their compositions (Tab. 6A and B) vary from tschermakites and magnesio-tschermakites (Al_2O_3 = 10.4–10.8 wt%, TiO_2 = 2.4–2.9 wt% and K_2O = 0.28–0.39 wt%) to magnesio-hornblende (Al_2O_3 = 7.8–8.8 wt%, TiO_2 =

Tab. 6 (A) Amphibole compositions in amphibole-plagioclase inclusions. (B) Amphibole compositions in rhyodacite. (Akrotiri volcanoes)

(A)	Cakro 11				Cakro 12			
wt%	core	rim	core	rim	core	rim	rim	rim
Sample No.	76	74	34	36	42	39	27	16
SiO_2	41.44	43.13	40.98	41.59	40.37	41.44	41.86	43.45
TiO_2	2.66	2.69	2.85	2.30	2.33	2.80	2.02	1.92
Al_2O_3	12.76	10.11	12.85	12.09	13.58	12.15	11.40	10.02
Cr_2O_3	0.02	0.04	0.04	0.06	0.04	0.05	0.07	0.06
Fe_2O_3	10.32	13.15	10.06	9.76	11.84	9.12	9.90	13.34
FeO	2.31	3.04	3.20	4.42	1.88	3.52	6.63	3.90
MnO	0.12	0.41	0.20	0.26	0.18	0.17	0.32	0.46
NiO	0.00	0.03	0.09	0.03	0.04	0.02	0.02	0.08
MgO	14.95	14.00	14.51	14.01	14.16	14.71	12.54	13.36
CaO	11.33	10.55	11.44	11.26	11.02	11.33	10.96	10.39
Na_2O	2.63	2.42	2.74	2.81	2.73	2.72	2.70	2.55
K_2O	0.19	0.17	0.21	0.20	0.22	0.21	0.22	0.16
H_2O	2.09	2.09	2.09	2.07	2.07	2.07	2.05	2.09
Total	100.83	101.84	101.25	100.88	100.44	100.31	100.69	101.77
xMg(Fe_{tot})	0.70	0.67	0.68	0.65	0.67	0.69	0.59	0.60
Name:	Mg-Hast	Mg-Hast	Mg-Hast	Mg-Hast	Mg-Hast	Mg-Hast	Mg-Hast	Tsch

(B)	Cakro 1		Bal 3			Rdch 1		
wt%								
Sample No.	200	215	C9	C5	C6	121	138	164
SiO_2	42.91	43.24	43.03	45.89	46.23	46.92	44.98	45.81
TiO_2	2.94	2.88	2.44	1.97	1.94	1.93	2.50	2.41
Al_2O_3	10.80	10.39	10.91	7.91	8.21	7.79	8.82	8.32
Cr_2O_3	0.04	0.06	0.01	0.00	0.00	0.01	0.05	0.05
Fe_2O_3	9.68	8.18	10.50	8.47	8.99	9.35	8.04	8.08
FeO	4.28	5.22	3.48	4.41	4.14	3.44	5.07	4.46
MnO	0.39	0.34	0.28	0.42	0.45	0.49	0.30	0.31
NiO	0.01	0.03	0.00	0.01	0.00	0.03	0.07	0.07
MgO	13.87	14.04	14.54	15.09	15.32	15.63	14.59	15.10
CaO	10.89	11.19	11.13	10.96	11.12	11.13	11.11	11.12
Na_2O	2.06	2.04	2.31	1.82	1.89	1.63	1.78	1.66
K_2O	0.39	0.34	0.28	0.31	0.33	0.29	0.36	0.33
H_2O	2.07	2.06	2.09	2.07	2.09	2.10	2.07	2.08
Total	100.33	100.01	101.00	99.33	100.71	100.74	99.74	99.81
xMg(Fe_{tot})	0.67	0.71	0.73	0.63	0.66	0.71	0.59	0.62
Name:	Tsch	Mg-Ho	Tsch	Mg-Ho	Mg-Ho	Mg-Ho	Mg-Ho	Mg-Ho

CAKRO 11, 12: Cape Akrotiri
BAL3: Cape Balos; lowermost rhyodacite pyroclastics
RDC1: C. Akrotiri; lowermost rhyodacite pyroclastics
Mg-Hst = Magnesio-hastingsite; Tsch = Tschermakite; Mg-Ho = Magnesio-hornblende

1.9–2.5 wt% and K_2O = 0.29–0.36 wt%), the latter ones as rims or microphenocrysts.

In contrast, the euhedral amphiboles within the xenolithic inclusions are magnesio-hastingsites (Fig. 7) with higher Al, Ti, Ni and Na but lower Mn and K contents than the amphiboles in the rhyodacites. They display strong brownish to red brownish pleochroitic colours. They often are normally zoned with Fe-enrichment towards the rims.

The hastingsitic amphiboles (Tab. 6A: Al_2O_3 = 12.7 to 13.8 wt%, TiO_2 = 2.6 to 2.8 wt%, Na_2O = 2.5 to 2.6 wt% and K_2O = 0.18 to 0.2 wt%) crystallised from water-rich melts of basaltic to andesitic composition. According to experimental data within tonalites, the stability field of similar amphiboles ranges from temperatures of up to 950 °C and pressures between 1 and 20 kbar (SCHMIDT, 1992). Using the $Al_{(tot)}$ content in the amphiboles and barometric calibrations (at approx. 700 °C, solidus temperatures), the crystallisation for the magnesio-hastingsites would take place at 20 to 25 km depths. However, this applies for a situation under the conditions of a buffered system with the mineral paragenesis amphibole, plagioclase, biotite, feldspar, quartz, titanite, Fe-Ti-oxides, melt and water. Deep-seated magma reservoirs, such as beneath Santorini, must be regarded as open, unbuffered systems. Thus, the stability fields of the amphiboles might have been rather different. In contrast to the magnesio-hastingsites it seems that the magnesio-hornblende in the rhyodacite with Al_2O_3 = 8 to 10 wt% may have crystallised during the ascent of the melts at lower pressures.

4.3. AMPHIBOLE DECOMPOSITION AND REACTIONS

Andesitic lavas and dikes often contain relics of hastingsitic amphibole xenocrysts, which show all steps of decomposition and reactions with the groundmass matrix or glass (Figs 8 and 9). These textural phenomena are also present in a sparse variety of magmatic inclusions (Type C: pseudocumulates), where the brownish groundmass glass has rhyodacitic to rhyolitic composition (Tab. 7).

The first step of decomposition (Fig. 8) is marked by dusty to black very fine grained Fe–Ti oxides (partly magnetite) starting from the rim (Fig. 8A), and at more advanced stages, by nucleation growth of the oxides, penetrating the whole crystal (Fig. 8B and 9). The euhedral shapes of the amphiboles show no distortion at these stages. This effect may only be attributed to syn- and post-eruptive oxidation and penetration by late

hydrothermal fluids and vapour. The following step (Fig. 8C) is marked by a decomposition reaction between the amphibole and the groundmass or former melts to produce fine grained aggregates of clinopyroxene, magnetite, melt and vapour. This step progressively leads to crystal growth of coarser clinopyroxene-magnetite aggregates, similar to metamorphic reactions producing cristalloblastic aggregates under ideal equilibrium conditions.

During the final step (Fig. 8D) the euhedral rims of the clinopyroxenes grow in equilibrium with the surrounding phases and the remaining melt. These reactions lead to fully recrystallised single crystals as well as to glomeroporphyritic clots of clinopyroxene, plagioclase and magnetite. Often, minor opacitic relics of amphibole can be recognised in the cores of well-shaped "pseudo-phenocrysts" of clinopyroxene.

The process may be explained either by complete mixing of early cumulate phases with partially remolten amphibole-rich cumulates with evolved rhyodacitic melts in deep-seated reservoirs, or during ascent and decompression of differentiated or hybrid basaltic and andesitic magmas.

Tab. 7 (A) Glass compositions in amphibole-plagioclase inclusions and rhyodacite lava (Cape Akrotiri). (B) Glass compositions of pumice and andesite/dacite lava (Capes Balos, Akrotiri and Mavro). (C) Glass compositions in glomeroporphyritic andesites (Cape Vounia).

(A)	Cakro 12/Inclusions in rhyodacite				Cakro 1/ Rhyodacite lava			
wt%	49	51	52	55	192	214	193	211
SiO_2	72.19	78.59	79.28	74.56	76.63	76.65	76.25	76.13
TiO_2	0.06	0.13	0.09	0.07	0.25	0.25	0.26	0.24
Al_2O_3	15.53	13.27	12.27	14.51	13.12	13.17	12.96	12.95
FeO	0.47	0.16	0.24	0.15	1.15	1.12	1.19	1.04
MnO	0.04	0.00	0.00	0.01	0.02	0.01	0.00	0.00
MgO	0.18	0.00	0.00	0.00	0.15	0.15	0.12	0.13
CaO	0.87	1.77	0.39	0.61	1.02	1.01	0.99	0.98
Na_2O	3.67	4.70	2.63	4.54	1.42	1.30	1.21	1.33
K_2O	4.42	0.67	3.69	3.52	2.14	2.57	1.97	1.95
Total	97.44	99.27	98.59	97.97	95.91	96.24	94.95	94.74

(B)	Bal 3/Rhyolite pumice			Rdch 1/Rhyolite pumice			Mavro 2/Lava andesite to dacite	
wt%	14	24	43	165	161	159	244	260
SiO_2	72.78	75.44	75.92	73.93	76.94	78.00	69.19	71.66
TiO_2	0.25	0.30	0.28	0.26	0.37	0.42	0.54	0.84
Al_2O_3	13.05	11.38	11.48	13.42	11.41	11.20	17.74	14.30
FeO	2.22	1.40	1.04	0.73	1.01	1.06	1.42	3.22
MnO	0.13	0.09	0.04	0.01	0.01	0.00	0.01	0.12
MgO	0.97	0.25	0.10	0.05	0.10	0.09	0.08	0.38
CaO	1.05	0.39	0.46	1.39	0.43	0.43	3.71	2.19
Na_2O	2.72	1.58	1.90	2.86	0.80	0.79	4.15	4.53
K_2O	3.23	4.02	3.81	2.18	2.49	2.47	2.20	1.78
Total	96.42	94.85	95.03	94.83	93.57	94.45	99.05	99.03

(C)	Cvun 7/Andesite lava				Cvun 1/Andesite lava			
	glass in cluster	glass in sieve plag	groundmass		brownish glass in cpx-plag-Fe-Ti oxide cluster			
wt%	192	171	126	128	266	268	270	271
SiO_2	67.65	71.90	72.60	72.97	71.77	71.97	70.22	71.62
TiO_2	0.42	0.83	0.88	0.71	0.90	0.81	0.82	1.02
Al_2O_3	17.70	12.25	12.64	12.27	13.03	12.65	13.31	12.18
FeO	1.37	2.73	2.13	2.32	2.43	3.08	3.19	3.52
MnO	0.05	0.04	0.05	0.01	0.04	0.05	0.07	0.04
MgO	0.12	0.27	0.26	0.15	0.15	0.18	0.28	0.35
CaO	3.33	1.03	1.28	1.14	1.20	0.93	1.16	1.16
Na_2O	4.38	0.84	1.37	1.20	1.53	0.72	0.81	0.63
K_2O	2.20	3.38	3.02	3.41	3.27	3.60	3.90	3.60
Total	97.22	93.27	94.22	94.19	94.32	93.98	93.76	94.12

5. Chemical composition of the Akrotiri volcanic rocks

55 samples of lavas, their inclusions and of pyroclastic components from the Akrotiri volcanoes have been analysed for a nearly complete range of major, minor and trace element compositions, listed in the Appendix, tables A1 to A3.

The bulk compositions of all Akrotiri lavas overlap entirely with the field of the "Main Santorini Volcanic Series" (Fig. 10). It is very significant that the andesites match in composition completely with the andesitic products (lavas, inclusions and pyroclastics) from the 1650 Columbos eruption (VOUGIOUKALAKIS and FRANCALANCI, 1996; VOUGIOUKALAKIS et al., 1996).

The chemical characteristics of the Akrotiri lavas and pyroclastics, which form a compositional range from basalt to rhyolite, are typical calc-alkaline, low to medium potassic trends in island arcs.

The rocks can be classified according to their differentiation index (D.I.: felsic normative minerals, Q + Or + Ab + Ne + Kp + Lc; THORNTON and TUTTLE, 1960) into basalts with < 30; basaltic andesites 35–50; andesites 50–65; dacites 65–80 and rhyodacites > 80. Another chemical approach using bulk chemical composition is the classification

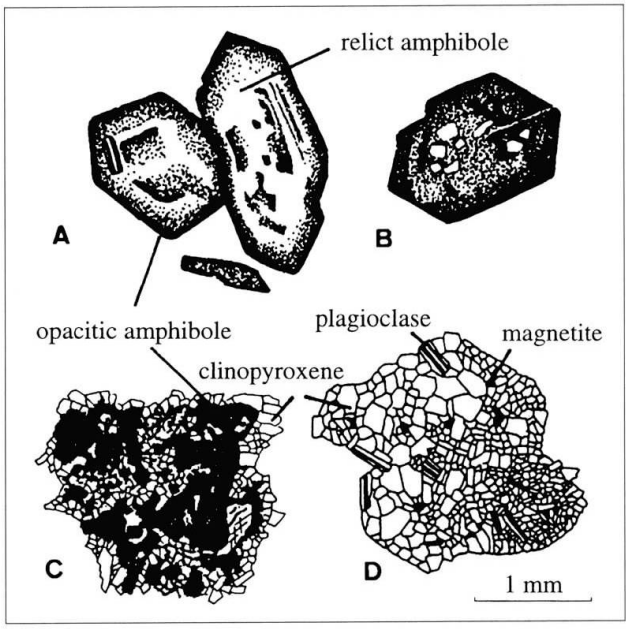

Fig. 8 Amphibole decomposition and reactions. A: Amphibole with opacitic rim of Fe–Ti oxide aggregates. B: Amphibole penetrated by opacitic Fe–Ti oxides. C: Decomposition and reaction of amphibole to form clinopyroxene-magnetite and melt plus vapor. D: Progressive crystal growth of clinopyroxene.

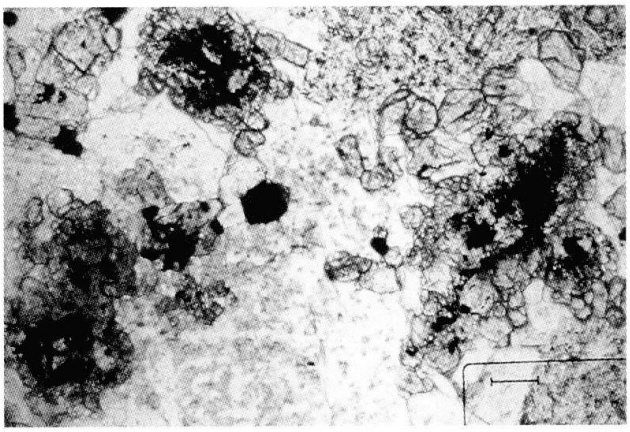

Fig. 9 Amphibole relics after decomposition and reaction in andesitic dyke from Mt. Loumaravi (Arhan 3). Reaction aggregates comprise clinopyroxene and magnetite. Figure size: 2.6 mm across.

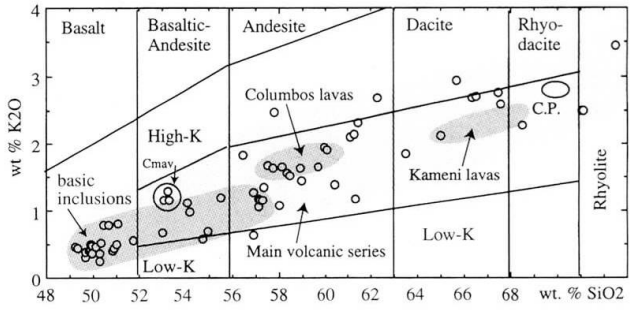

Fig. 10 Bulk chemical composition (SiO_2 vs K_2O in wt%) and classification of the Akrotiri volcanics compared to the "Main volcanic series" of Santorini, the Kameni lavas and to the Columbos 1649/50 eruptive products. C.P. = Columbos pumice (data from NICHOLLS, 1971; HUIJSMANS et al., 1988; VOUGIOUKALAKIS and FRANCALANCI, 1996).

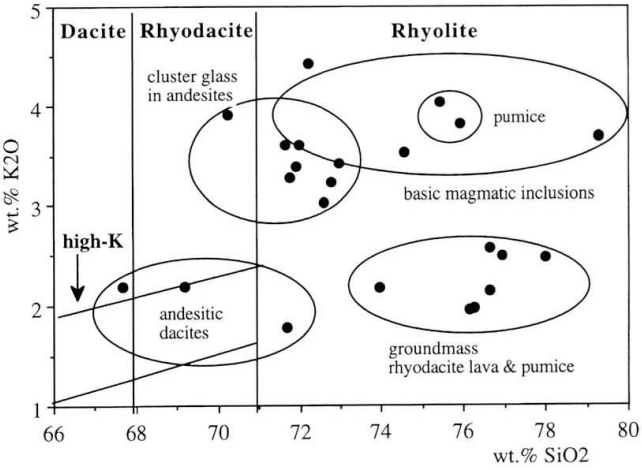

Fig. 11 Glass compositions within the Akrotiri volcanics.

of PECCERILLO and TAYLOR (1976), figure 10. Such a nomenclature does not take into account the high amount of xenolithic material within the rhyolites, rhyodacites and dacites, which shifts the chemical bulk composition and, therefore the differentiation index towards apparently more basic compositions.

The overall chemical compositions and variations of the Akrotiri lavas and pyroclastics are mainly controlled by fractional crystallisation of the observed phenocryst phases olivine, plagioclase, clinopyroxene, amphibole, Ti-magnetite and apatite as well as by variable processes of magma mixing (chemical homogenisation) and magma mingling (mechanical blending).

Figure 11 shows the glass compositions of lavas and pumice. The difference between the average total wt% of oxides of these glasses and 100% ranges between 4 and 6%, which is interpreted to be due to volatiles dissolved in the glass. This gives a first estimate about the water content in the Akrotiri magmas. Two major groups of glasses can generally be distinguished: glasses with low- to medium K and glasses with high-K concentrations. The groundmass glasses (Fig. 11) of the rhyodacitic lavas indicate the general differentiation trend, expressed in the bulk chemical composition of the lavas. Therefore, these glasses represent the ultimate residual liquids of the Akrotiri magmatic series. The groundmass glasses of the andesitic dacites (e.g. those from Cape Mavro) have more basic concentrations, indicat-

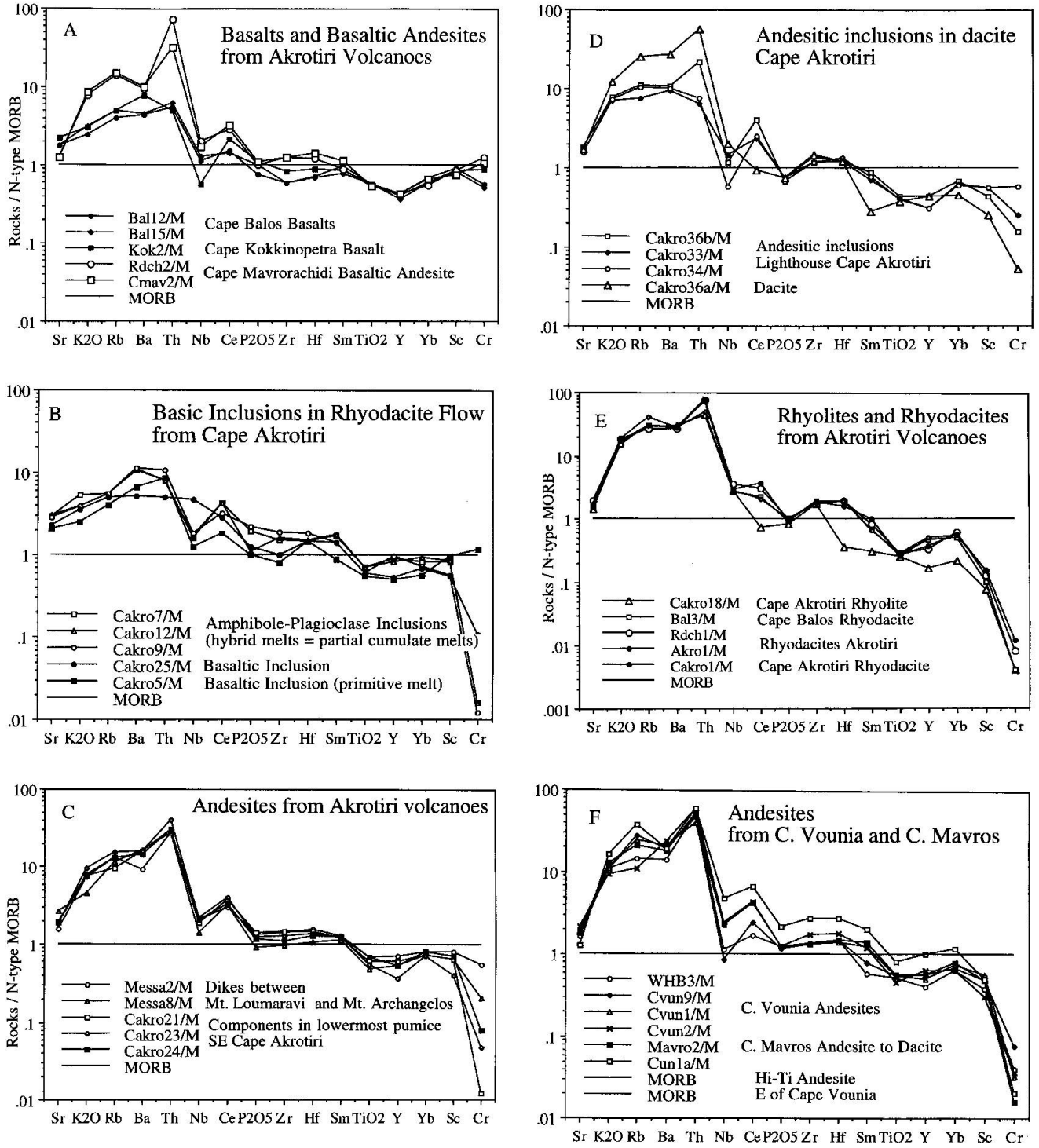

Fig. 12 Spider diagrams of the bulk chemical composition of the Akrotiri volcanic rocks, normalised to normal N-type Mid-Ocean Ridge (MORB) basalt composition (SUN et al., 1979; PEARCE, 1982; SAUNDERS and TARNEY, 1984).

ing magma mixing effects between andesitic and rhyodacitic magmas. In contrast, the high-K glasses are distributed in the plagioclase/clinopyroxene/magnetite clusters and inclusions in plagioclase macrophenocrysts of the glomeroporphyritic andesites, as well as in the interstices of the porous amphibole/plagioclase basic inclusions. These glasses appear to be the products of reactions between cluster phenocrysts and their surrounding melts (Fig. 8D). They also represent residual liquids. This is the case in the basaltic to andesitic magmatic inclusions, which were formed by undercooling and quenching during the ascent into rhyodacitic magmas. Therefore, each inclu-

sion has to be regarded to as a small isolated magmatic system, rapidly crystallising amphibole / plagioclase / magnetite assemblages and leaving highly differentiated residual liquids behind (Fig. 7).

The general chemical characteristics of the Akrotiri lavas and their inclusions are summarised in figure 12 (spider diagrams). The selected diagnostic major and trace element compositions are normalised against normal-type "Mid Ocean Ridge Basalt" (N-MORB).

The basalts of Cape Balos and Cape Kokkinopetra can be classified as high alumina olivine basalts with typical island arc characteristics (IAT). They are enriched up to ten times in the more-hygromagmatophile or low field strength elements (LFS) such as K, Rb, Ba, Th, U, and the light rare earth elements (LREE) as well as to a lesser extent Sr, Hf and Zr. In contrast, the basalts are depleted in the less-hygromag-mathophile or high field strength elements (HFS), such as Nb, Ti, Y, and the heavy rare earth elements (HREE).

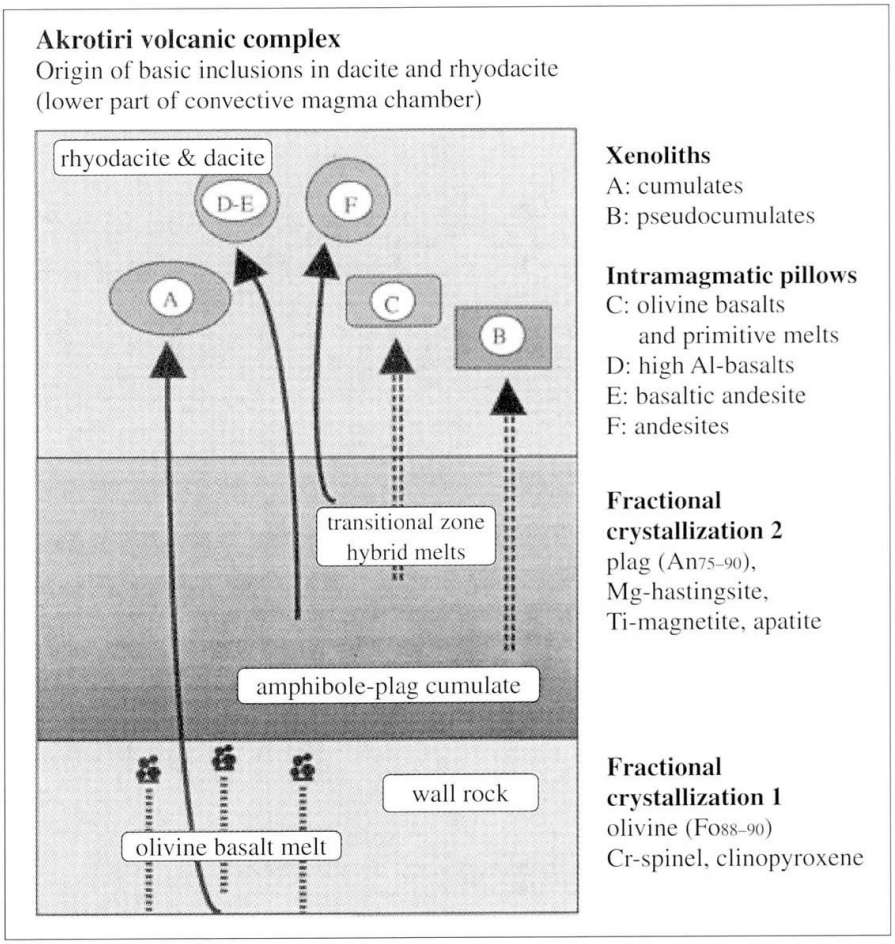

Fig. 13 Differentiation processes in the Akrotiri volcanic complex. Model of amphibole- and plagioclase-dominated fractional crystallisation and the origin of basic xenolithic inclusions in silicic magmas within deep-seated crustal magma reservoirs.

The patterns of the basalts and inclusions are very similar, which shows the close magmatic relationship between the basaltic magmas reaching the surface and their inferred counterparts from the magma reservoirs.

The compositions of the intermediate and evolved lavas, such as the dacites and rhyodacites are enriched up to hundred times MORB.

Positive correlation of K, Rb and Ba with Th is evident. This also holds for Nb, Zr, Hf, Ta, U and the LREE, whereas the compatible minor and trace elements Cr (incl. Ni, Co), V, and Sc display a negative correlation with Th. In this respect, the Akrotiri lavas do not significantly differ from the younger "Main Volcanic Series" on Santorini (NICHOLLS, 1971 and 1978; MANN, 1983; BARTON and HUIJSMANS, 1986; MITROPOULOS et al., 1987; HUIJSMANS et al., 1988; FYTIKAS et al., 1990; KALOGEROPOULOS and PARITSIS, 1990).

However, all Akrotiri volcanic rocks have much lower concentrations in the hygromagmatophile elements than the equivalent volcanic rocks in all other islands of the Aegean arc (Aegina, Poros and Methana: DIETRICH et al., 1988; Kos and Nisyros, GUELEN et al., 1987; WYERS and BARTON, 1989; GUELEN, 1990). Using Sr/Th variations, the Akrotiri lavas and pyroclastics show very little crustal contamination (BRIQUEU et al., 1986).

At a closer look, chemical irregularities appear within the intermediate volcanics, the basaltic andesites, andesites, andesitic dacites, and dacites (Figs 12 A, C, D, and F) for K, Rb, Ba, Nb, REE, P, Zr, Hf, Ti, Y, Sc and Cr. These features cannot be explained by simple fractionation processes of anhydrous phases (i.e. plagioclase, pyroxenes, olivine, magnetite and apatite) from basalt to rhyodacite, as proposed for the "Main Volcanic Series" (MANN, 1983). The early crystallisation of plagioclase, amphibole and Ti-magnetite together with clinopyroxene is evidence for a discontinuous differentiation process leading to evolved rhyodacitic melts.

The spider diagrams exhibit these characteris-

tics very clearly. Extreme fractional crystallisation is indicated in the Akrotiri rhyolite (Fig. 12E), expressed by the depletion of most of the rare earth elements, Sc and Cr.

In addition, magma mixing processes, generated by replenishment of primitive basaltic melts into a pre-existing magma reservoir with evolved melt have to be envisaged, in order to explain other bulk chemical irregularities. Magma mixing can explain the basaltic andesites of Cape Mavrorachidi (Fig. 12A), while mechanical mixing (mingling) can be seen in the spider diagrams of andesites, andesitic dacites, dacites, and rhyodacites (Fig. 12 C, D, and F).

6. Magmatic processes in the Akrotiri Volcanic Complex (3-step model)

DAVIS et al. (1996) has previously introduced the evolution of the Akrotiri Volcanic Complex and its magmatic processes. The lower Akrotiri volcanic sequence, which started mainly with silicic magmas and continued with the production of heterogeneous dacites, ended with andesites. After a period of magmatic quiescence, andesites and dacites appeared again followed by high alumina basalts and basaltic andesites. The inverse occurrence of eruptive products within the Akrotiri complex can be explained by a series of complex magmatic processes (DAVIS et al., 1996; DIETRICH et al., 1996; GARTZOS et al., 1996):

A 3-step model (Fig. 13) is proposed to illustrate the magmatic evolution of the Akrotiri Volcanic Complex. Steps I and II represent the major magmatic processes for the generation of the Akrotiri magmas, while step III is only regarded to as a process within magma reservoirs of greater crustal depths, maybe even close to the mantle/crust boundary. The latter mechanism may help to explain the basic magmatic inclusions within evolved dacitic and rhyodacitic magmas as injected and quenched (pillowed) hybrid melts. It is also regarded as the fundamental trigger within an instable, stratified magma reservoir leading to its turnover, degassing and ascent of the melts to a shallow crustal reservoir or to the surface.

6.1. STEP I: FRACTIONATIONAL CRYSTALLISATION

6.1.1. Early crystal fractionation

Early fractional crystallisation led to the formation of olivine basalts from an inferred primary, calc-alkaline basaltic melt.

The primary composition of the basaltic magmas has been discussed previously (NICHOLLS, 1971 and 1978; BARTON and HUIJSMANS, 1986). A primitive basaltic composition was derived by adding 12 wt% olivine (Fo_{90}), 4 wt% clinopyroxene and 0.5 wt% Cr-spinel to the least evolved basalt (NICHOLLS, 1978). A similar primitive basaltic composition is used in the proposed fractional crystallisation model as starting melt composition, which has been calculated by adding olivine, clinopyroxene and Cr-spinel to the average Balos basalt composition (DIETRICH et al., 1996). Tracers of this process are forsterite-rich olivine and Cr-spinel xenocrysts in the high alumina basalts. The early olivine (Fo_{90}) phenocrysts must have formed from a water-bearing, primitive low-Ti basaltic melt (xMg = 0.74, K_2O = 0.5 wt%, TiO_2 = 0.8 wt%, Ba = 80 ppm, La = 6 ppm, Eu = 15 ppm, Yb = 2 ppm, Y = 10 ppm, Sc = 35 ppm). Besides olivine and Cr-spinel, minor amounts of clinopyroxene must have been involved in this fractionation process:

Primary basaltic melt (xMg = 0.73–0.74)
– (olivine, clinopyroxene, Cr-spinel)
= high alumina basalt (xMg = 0.70)

6.1.2. Amphibole – plagioclase fractional crystallisation

The main crystal fractionation is marked by the crystallisation of Al, Ti, Na and K-rich Mg-hastingsitic amphibole, clinopyroxene, plagioclase (An_{90-85}), and magnetite:

High Al-basalt
– (plagioclase, clinopyroxene, amphibole, Ti-magnetite)
= rhyodacite

The depth of fractional crystallisation can only be estimated from experimental studies. Hastingsitic amphiboles seem to be rather stable at high pressures and temperatures since they all show signs of decomposition and reaction during ascent into shallow reservoirs or to the surface. This implies deep crustal conditions for their original crystallisation, probably close to the mantle-crust boundary. The extraction of these minerals, in particular amphibole with its complex composition, drastically changes the composition of the remaining melt by extracting Mg, Ti, Fe, Al, Ca and other elements, leaving a depleted but silica-enriched rhyodacitic melt.

Model calculation
High Al-basalt
– (plagioclase, clinopyroxene, amphibole, Ti-magnetite)
= rhyodacite

Fractional crystallisation can also be defined as a mixing process, and therefore can be treated by using a two-stage computer based calculation (WRIGHT and DOHERTY, 1970).

The rhyodacitic magmas are a result of crystallisation of Fo-rich olivine (+ chromian spinel), An-rich plagioclase, augite, amphibole and titanomagnetite from water bearing basaltic melts (Tab. 8). A primitive basaltic composition with island arc tholeiitic (IAT) affinities was chosen for the mixing calculations, listed in table 8 (low in K_2O = 0.6 wt%, TiO_2 = 0.9 wt% but high in MgO = 11.98 wt%).

The mixing calculations (Tab. 8) show that the calculated basaltic composition is very similar to the input basaltic composition. 21 wt% of evolved rhyodacitic magma can be derived by discontinuously fractionating approximately 60% cumulates, composed mainly of amphibole-plagioclase and smaller amounts of olivine (15%). Here, we have to admit that for the olivine only an average composition of Fo_{83} was chosen, which gives the best solution. A more precise solution can be obtained involving a series of calculations with small differentiation intervals and starting fractionating olivine Fo_{90}.

Tab. 8 Amphibole fractionation model. Input data: primitive melt (DIETRICH et al., 1996); amphibole and plagioclase from coarse grained basic inclusion Cakro 11 in rhyodacitic matrix Cakro 18; calc. comp. = calculated basaltic composition after least square fitting.

	calc. comp.	prim. melt	amphibole Cakro 11	plag. An_{86} Cakro 11	oliv. Fo_{83}	rhyodacite Cakro 18
wt%						
SiO_2	48.55	50.02	41.56	46.48	39.32	72.60
TiO_2	0.96	0.89	2.40	0.04	0.00	0.38
Al_2O_3	16.97	16.23	13.98	33.72	0.00	14.32
FeO	7.84	8.07	12.91	0.64	16.42	2.40
MnO	0.12	0.12	0.19	0.04	0.20	0.04
MgO	11.98	11.90	14.58	0.07	43.91	0.30
CaO	9.29	9.65	11.35	17.47	0.15	2.60
Na_2O	2.44	2.52	2.81	1.53	0.00	4.82
K_2O	0.62	0.61	0.23	0.01	0.00	2.54
Total	98.78	100.00	100.00	100.00	100.00	100.00
Solutions wt%	99.00		36.00	26.00	15.00	21.00

Bulk chemical trace element modelling

The compositions of 12 selected basic xenoliths from rhyodacites of Cape Akrotiri are listed in Appendix, table A3. These porous acicular inclusions belong mainly to D, E and F types with chemical compositions from differentiated, low Mg high-alumina basalt to basaltic andesite. One inclusion (Cakro 5) with normal basaltic composition is also shown (type A). The chemical characteristics are expressed with the help of spider diagrams normalised to N-type MORB in figure 12B. These inclusions derived from slightly saturated (hypersthene normative) melts which were already enriched in the more-hygromagmatophile elements but highly depleted in Mg, Cr and Ni with respect to the olivine basalt lavas of Cape Balos and Cape Kokkinopetra.

In order to demonstrate the fractional crystallisation of amphibole, plagioclase and magnetite from basaltic melts in terms of their bulk chemical composition, two diagrams have been chosen (Figs 14 and 15). Cakro 5 represents the composition of olivine basalt melt, similar to the composition of the Balos basalts. The very coarse-grained amphibole-plagioclase inclusions Cakro 9 and 12 (type D) are so far the best candidates to

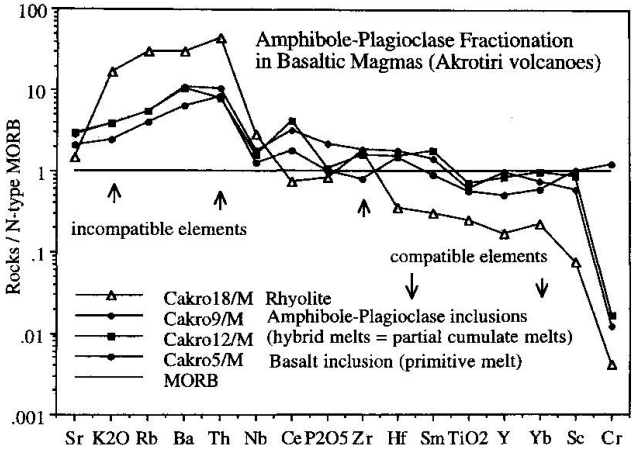

Fig. 14 Amphibole-plagioclase fractionational crystallisation in Akrotiri basaltic magmas. Normalisation to N-type Mid-Ocean Ridge (MORB) basalt composition (SUN et al., 1979; PEARCE, 1982; SAUNDERS and TARNEY, 1984).

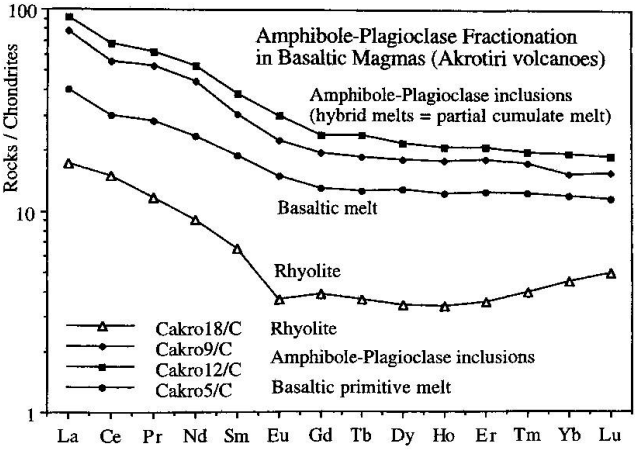

Fig. 15 Amphibole-plagioclase fractionation in Akrotiri basaltic magmas; displayed in the rare earth element (REE) distribution patterns. Normalisation to C1-chondrites (EVENSEN et al., 1978).

represent cumulate compositions. The latter selection is based on the assumption that these inclusions crystallised from vapor-rich hybrid basic melts, which were derived by partial melting of amphibole- and plagioclase-rich cumulates.

The following conclusions can be drawn from the two diagrams (Figs 14 and 15). During fractional crystallisation of amphibole, plagioclase, magnetite and to a minor amount clinopyroxene and apatite, the incompatible elements (K, Rb, Ba, Th, and to a lesser extent Zr) are portioned into the evolved rhyodacitic to rhyolithic melts. All rare earth elements, Sr, Hf, Ti, Sc and Cr behave compatibly, being drastically extracted from the melt by the crystallisation of the cumulate phases.

The inclusions chosen do not represent ideal cumulates. The 10 to 15% enrichment of K, Rb, Ba, LREE, Hf and Th can be attributed to the mixing process of the partially molten cumulates with rhyodacitic melt prior to or during injection of the hybrid melts into the rhyodacitic magmas. The enrichment of Ti, Y and HREE accounts for the incorporation of these elements into the mafic cumulate phases.

6.2. STEP II: GENERATION OF DACITES BY MINGLING PROCESSES (MECHANICAL MIXING)

The dacites built up large volumes during both volcanic cycles in the Akrotiri volcanic complex. All dacites contain variable amounts of basic magmatic inclusions and xenocrysts. The macroscopic diversity goes down to microscopic scale. Small sized (1–5 mm) magmatic inclusions and xenocrysts occur in a rhyodacitic matrix. The xenocryst compositions in the dacites are identical with the minerals fractionated in the second step, whereas the phenocrysts compositionally match the phenocrysts from the rhyodacites. Only weak normal zonations are recorded in the macrophenocrysts (amphibole and plagioclase). The complex textural diversity of the dacites is also reflected in the bulk chemical composition, which changes from one extrusion site to another, and often within one flow or plug.

Mingling of xenocrysts and magmatic inclusions with the rhyodacitic melt can derive spread in the bulk chemical variation from andesitic dacites through dacites to rhyodacites. Least-square modelling (not shown in this paper) has been utilised to test all steps of mingling. The process of mingling is regarded to as a mechanical process, which can be achieved during turnover in the stratified magma chamber (Fig. 13).

6.3. STEP III: MAGMA MIXING

Magma mixing is understood as a homogenisation process involving at least two magmas of different chemical compositions and rheologies (McBIRNEY, 1980). Such a process can occur under the following conditions:

- Replenishment of a pre-existing magma reservoir containing differentiated melts with new basaltic melt;
- turnover of an instable zoned or layered magma reservoir filled with chemically and rheologically different melts;
- during ascent and emplacement of compositionally different magmas;
- during multiple intrusion and cooling of melts at shallow crustal depths (i.e. dike swarms).

In island arc and continental margin environments, replenishment of magma reservoirs with hot undifferentiated melt and magma mixing seem to be common phenomena and have been intensively discussed (e.g. EICHELBERGER, 1975; EICHELBERGER et al., 1985; KOYAGUSHI, 1986; FEELEY and DUNGAN, 1996). In addition, a significant melting process may accompany these mixing processes. OBERHÄNSLI et al. (1985 and 1989) and DIETRICH et al. (1986) have described partial melting effects of cumulates, observed in magmatic inclusions in basaltic andesites and andesites from Aegina and Methana. These coarse-grained amphibole/plagioclase cumulates show signs of partial melting, probably initiated by injection of hot basaltic melts into cumulate-rich magma reservoirs and generating small portions of hybrid, water-rich, foamy melts of basaltic to andesitic composition.

6.3.1. Incomplete magma mixing

If magma mixing was incomplete and rapid cooling or quenching of the melts occurred, then the mixing process can still be recognised by the existence of unmixed portions of the different magmas or in different phenocrysts compositions; i.e. inverse zonation or compositional gaps.

However, it is difficult to reconstruct such a mechanism, if the process was nearly complete. Only the chemical modeling using bulk rock composition, phenocryst compositions and isotopic ratios remain as useful tools.

In the case of intermediate volcanics in the "Akrotiri Volcanic Complex", the first description of incomplete magma mixing by FOUQUÉ (1879) is a classical example (Fig. 16). A dike south of Mt. Loumaravi clearly shows mixing phenomena of three compositionally different types of basic to

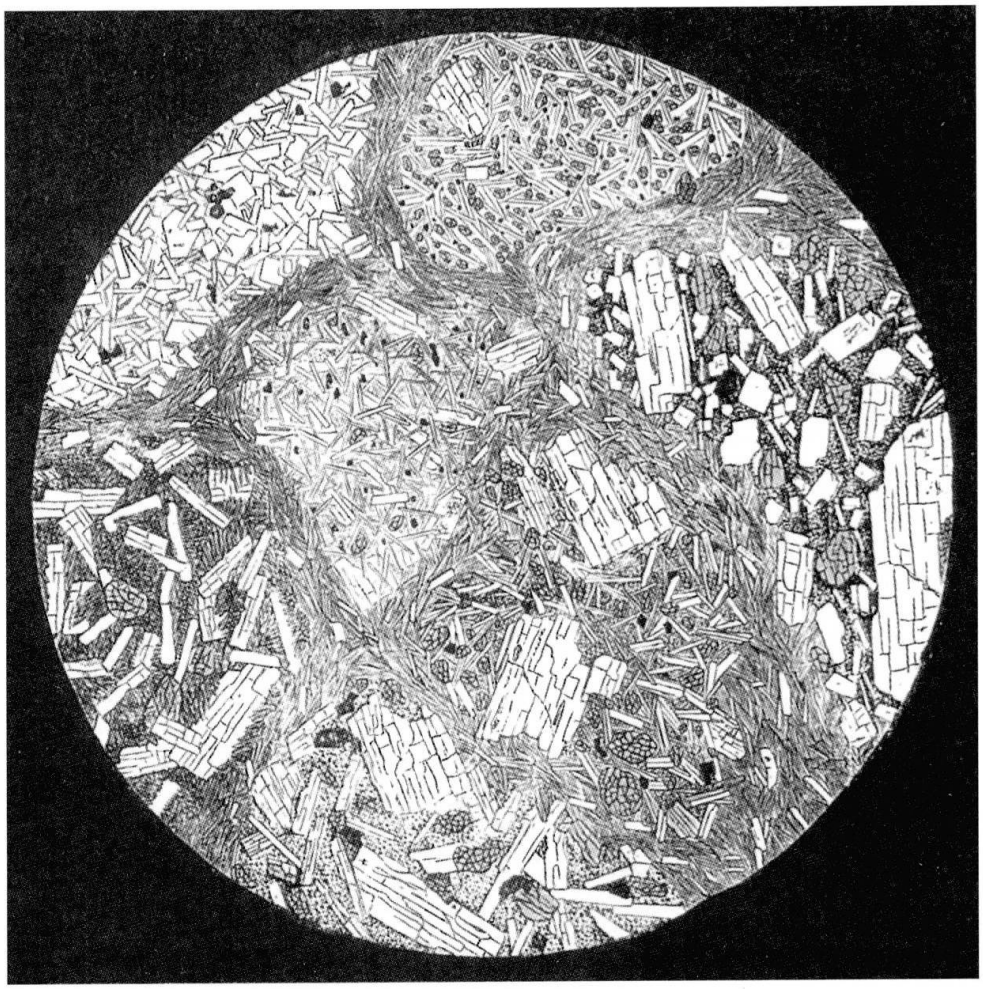

Fig. 16 Incomplete magma mixing in a basaltic andesite dike from Mt. Loumaravi; photomicrograph from FOUQUÉ (1879), crossed polars, figure size approx. 10 mm across.

intermediate melts: a glass-rich, clinopyroxene bearing dacitic melt, a glass- and plagioclase-rich andesitic melt and a fine-grained plagioclase/clinopyroxene basaltic melt with eutectic (intersertal) textures. All three components are embedded into an interstitial pilotaxitic plagioclase-rich, high-alumina basaltic melt. Similar phenomena have been reported from basaltic andesites of the Skaros volcano in the much younger "Main Volcanic Series" of Santorini (HUIJSMANS and BARTON, 1983; WYERS et al., 1987; HUIJSMANS et al., 1988).

6.3.2. Complete magma mixing

Partial melting by replenishment of primitive basaltic melts into magma reservoirs and complete magma mixing can explain the appearance of the small volumes (~ 5% of the total volcanic edifice) of high-alumina basalt, basaltic andesite and hypersthene bearing andesite during the first volcanic cycle of the Akrotiri complex.

The basaltic andesites and andesites exhibit typical features of resorption, decomposition, reactions and melting of amphibole and plagioclase (see chapter 4, Fig. 8). In the andesites, amphibole is not a phenocryst phase but always a Mg-hastingsitic xenocryst phase partly transformed into black opacitic aggregates. The amphiboles show all steps of resorption and reaction from Mg-hastingsite (in some cases) including forsteritic olivine to diopsidic augite, magnetite, plagioclase, and glass. Further reaction leads to the recrystallisation of these clinopyroxene aggregates to form clinopyroxene "pseudo-phenocrysts". The groundmass phenocrysts are andesine, hypersthene and olivine (Fo_{65}) in a groundmass glass of dacitic to rhyodacitic composition.

6.4. MAGMA MIXING BETWEEN BASALTIC AND ANDESITIC MELTS: THE GENERATION OF THE CAPE MAVRORACHIDI BASALTIC ANDESITE

Simple magma mixing also occurred in the Akrotiri Volcanic Complex, involving two end-member melt compositions besides complex mixing processes such as partial melting of cumulates or incomplete mixing due to periodic replenishment and turnover of magma reservoirs.

6.4.1. Model calculation

The hypersthene bearing andesites of the second volcanic cycle (i.e. those at Cape Mavrorachidi) are in texture and mineral compositon fairly ho-

mogeneous and show only a few almost completely resorbed amphibole relics. These features cannot be explained by simple fractional crystallisation of olivine, spinel, clinopyroxene and plagioclase from a primitive basaltic melt alone, but by a simple mixing process between pre-existing dacitic melt with an olivine basalt magma (DIETRICH et al., 1996). This can be demonstrated by compositional gaps in the macrophenocrysts of plagioclase and clinopyroxene. Although minor amounts of older plagioclase xenocrysts occur, we assume two endmember melt compositions to be responsible for the mixing process, olivine basalt magma from Cape Balos and andesitic to dacitic melts similar to that from Cape Mavros.

Major-element modelling (using the least-square calculation program by WRIGHT and DOHERTY, 1970) of binary mixing of basalt from Cape Balos with andesitic dacite was performed in order to test the assumption of magma mixing in the Cape Mavrorachidi basaltic andesites. The bulk chemical compositions of these volcanic rocks are listed in the Appendix, table A1. A small percentage of olivine (Fo_{86}) had to be added to the average basalt composition. The calculation (Tab. 9) clearly shows that approximately two thirds of basaltic melt and one third of andesitic to dacitic melt is required to produce the basaltic andesites of Cape Mavrorachidi.

Tab. 9 Magma mixing model. Input data: bulk rock compositions of basaltic andesite Cmav 3, ol-basalt Bal 15 and andesite Mavro 4; calc. comp. = calculated basaltic andesite composition after least square fitting.

	calc. comp.	basalt. and Cmav 3	ol-basalt Bal 15	olivine Fo_{86}	andes. dac. Mavro 4
wt%					
SiO_2	53.75	53.93	49.91	39.45	62.36
TiO_2	0.78	0.81	0.86	0.03	0.70
Al_2O_3	16.50	16.01	17.65	0.03	16.14
FeO	7.32	7.57	8.11	13.26	5.22
MnO	0.13	0.14	0.15	0.21	0.08
MgO	7.45	7.44	7.58	46.83	2.96
CaO	8.94	9.11	11.22	0.19	5.65
Na_2O	4.07	3.82	3.94	0.00	4.73
K_2O	1.08	1.16	0.56	0.00	2.15
Total	100.02	100.00	100.00	100.00	100.00
Solutions wt%	100.20		62.54	3.64	33.84

6.4.2. Bulk chemical trace element modelling

Magma mixing processes can also be demonstrated with the help of trace element modelling. Normally, variation diagrams or ratio-ratio plots, considering incompatible ratios such as Zr/Y vs K/Rb or Rb vs Rb/K are used. These plots, although not

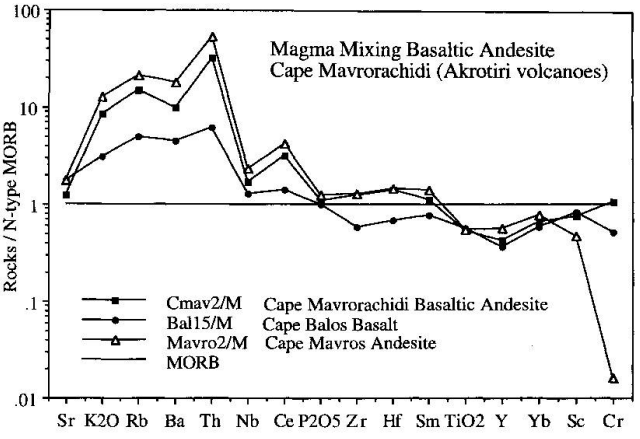

Fig. 17 Magma mixing in Cape Mavrorachidi basaltic andesite. Normalisation to N-type Mid-Ocean Ridge (MORB) basalt composition (SUN et al., 1979; PEARCE, 1982; SAUNDERS and TARNEY, 1984).

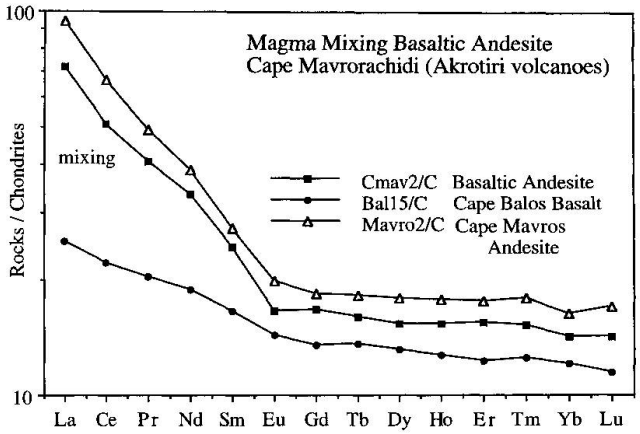

Fig. 18 Magma mixing in Cape Mavrorachidi basaltic andesite displayed in the rare earth element (REE) distribution patterns. Normalisation to C1-chondrites (EVENSEN et al., 1978).

given here, show hyperbolic data distributions, typical of mixing trends. In order to involve as many elements as possible, the normalised "spider diagram" (Fig. 17) and the normalised rare earth distribution diagram (Fig. 18) have been chosen.

On the spider diagram, almost all elements, incompatible as well as compatible, clearly show mixing in the basaltic andesites of Cape Mavrorachidi. The minor differences in Sr, P and Ti may be explained in sampling artefacts, i.e. spatial distribution of apatite, Fe-Ti-oxides and small amounts of plagioclase xenocrysts in the andesitic dacites and in the basaltic andesites. The relatively higher Cr contents compared to Balos basalt indicates that the endmember of olivine basaltic composition should have had higher chromium

content. This effect already appeared in the major element mixing calculation, where a small amount of 3.6 wt% of olivine was added, in order to fit the perfect binary mixing. In contrast, the rare earth element distribution patterns (Fig. 18) unambiguously show mixing.

7. Discussion

7.1. ORIGIN OF BASALTIC MELTS AND DEPTH OF MAGMA RESERVOIRS

The discussion about the source of the Akrotiri basaltic magmas will be related to the existing literature about Santorini (NICHOLLS, 1978; HUIJSMANS et al., 1988). All data, especially the trace element compositions (e.g. those of Ta, Th, Hf, U) and the rare earth elements, suggest for the primary Akrotiri basaltic magma a very similar source as for the basaltic magmas of the "Main Volcanic Series".

The primary high alumina basaltic melts may have originated by a large percentage of partial melting from a rather depleted mantle wedge at approximately 120 to 130 km depth. Such a mantle is enriched in water and in hygromagmatophile elements K, Rb, Ba, Sr, Th, U, and LREE, derived from the breakdown of subducted high-pressure phases antigorite, phlogopite etc. from altered and metamorphosed oceanic crust (ULMER and TROMMSDORFF, 1995). During ascent through the lithosphere, the primary magmas underwent high-pressure fractional crystallisation of olivine, clinopyroxene and Cr-spinel under open system oxygen buffered conditions (OSBORN, 1976; OSBORN and RAWSON, 1980).

Mg-rich hastingsitic amphibole and anorthitic plagioclase are present in various proportions as the two major xenocryst phases in most of the Akrotiri lavas, and therefore appear to be important "magmatic index fossils" with respect to the chemical irregularities observed in the intermediate volcanics and the fractional crystallisation processes. The crystallisation of plagioclase, amphibole and Ti-magnetite together with clinopyroxene manifests a discontinuous differentiation process leading to evolved rhyodacitic melts. In addition, magma mixing and mechanical mingling processes have been recognised within the Akrotiri volcanics to play important roles in the generation of dacites and hybrid andesites.

Amphiboles, in particular hornblende, tschermakite and hastingsite, crystallise within a large stability field, ranging from approximately 2 kbar at 1025 °C (SISSON and GROVE, 1993 a and b) to high-pressures between 10 and 18 kbar (ALLEN et al., 1975; ALLEN and BOETTCHER, 1978; SEMET and ERNST, 1981). These results would explain the disappearance of amphibole in high-crustal magma chambers. The depths of reservoirs at deeper crustal levels are still in dispute. Experimental studies on Santorini basalts and basaltic andesite (OSBORN and RAWSON, 1980) suggest crystallisation of the observed anhydrous phases plagioclase, augite, olivine and magnetite in deep-seated magma reservoirs > 30 km, close to the base of the Aegean crust. In the Akrotiri lavas, a compositional gap between magnesio-hornblende and tschermakitic hornblende in the rhyodacites and the magnesio-hastingsites in the basic inclusions and pseudocumulates exists, which lacks experimental explanation. The best argument for crystallisation of amphiboles at greater depths comes from the composition of the whole volcanic edifice and its structural characteristics. The oldest andesitic to rhyodacitic Akrotiri lavas which contain amphibole-rich inclusions are not associated with thick pumice deposits and lack large caldera structures. This feature is equivalent with the volcanic edifices on the islands of Aegina, Poros and Methana.

The volcanologic and petrologic evidence for deep seated magma chambers and rapid ascent of magmas through the crust is also supported by $^{87/86}Sr$, $\delta^{207/204}Pb$ and $\delta^{143/144}Nd$ isotopic ratios (GUELEN et al., 1987; WYERS et al., 1987; MITROPOULOS et al., 1987), which indicate very little signs of crustal contamination.

7.2. MAGMATIC AND VOLCANIC EVOLUTION OF THE AKROTIRI VOLCANIC COMPLEX

The Akrotiri Volcanic Complex represents the early stages of volcanic evolution of the Santorini volcanic islands. Field evidence shows that no clear remnants of an old large caldera structure within this complex exist. The flows and pyroclastic deposits were mainly deposited subaerially from fissures and cinder cones, later filled with necks and plugs. In a few cases they erupted within submarine environment.

The beginning of volcanic activity can only be estimated from volcanic detritus in the upper Pliocene volcanoclastic sediments. No other volcanic relics have been found from this early period.

The lower part of the Akrotiri volcanic edifice is formed by dacitic to rhyodacitic flows, pumice layers, pyroclastic and epiclastic flows which were subsequently intruded by numerous andesitic dikes. Amphiboles are the most common mafic minerals in these volcanic rocks. They occur as

pheno- and xenocrysts in rhyodacites, dacites and andesites and exhibit a large variation in mineral chemistry from Mg-rich hastingsite through evolved hastingsite to hornblende.

The early stages of the silicic volcanic activity in the Akrotiri complex ended with a magmatic pause accompanied by extensive uplift and erosion leading to peneplanation of the Akrotiri area. The exact timing is still unclear, but it may have occurred around 600'000 to 500'000 years ago.

Magmatic reactivation started with the eruption of amphibole-free andesites and dacites and terminated with the appearance of basalts and basaltic andesites along N–S trending fault zones. It can only be assumed that a tensional tectonic regime took over in the southern Aegean arc and back arc region, due to major changes of the Mediterranean plate motions, leading to horst-graben structures (e.g. the Christiana-Santorini-Amorgos ridge). A new SW–NE trending lineament with perpendicular tensional movements parallel to the Andros basin and the Santorini-Anafi graben system seems to have developed (PERISSORATIS et al., 1996). This major tectonic change may have caused decompression on the mantle beneath the Santorini islands, leading to upwelling of the asthenosphere and thinning of the subcontinental lithosphere, increasing the volume and degree of partial melting.

Along the intersection between the Plio-/Pleistocene N–S fault system and the younger SW–NE faults, larger volumes were able to rise from greater crustal depth to the surface. The major change of the tectonic regime was also accompanied by a northward shift of the volcanic eruption centres; (Fig. 1), expressed even in the recent volcanic activity of the Kameni and Columbos volcanoes.

This whole process could also explain both the smaller magmatic volumes within the Akrotiri volcanic complex and the crystallisation of amphiboles at deep crustal reservoirs. This is due to a thicker lithosphere prior to the tectonic change, and the appearance of large volumes of the younger "Main Volcanic Series" and their continuous fractional crystallisation processes after that change. The four major rhyodacitic pumice eruptions and large caldera collapses require at least six times their erupted volumes of primitive basaltic magmas, at least an order of magnitude of several 100 km^3.

The major conclusion for the generation of the Akrotiri magmas can be drawn from the appearance of amphiboles within the rhyodacites and dacites as well as from their basic amphibole-plagioclase inclusions. Amphibole crystallisation seems to be controlled by the presence of water-rich basaltic melts as well as by a large stability field within thick sialic crust. The variable depths of the magma reservoirs have to be assumed according to the stability fields of different amphibole compositions.

Therefore, discontinuous fractionation processes involving large quantities of amphibole might have taken place at great crustal depth, leading to evolved rhyodacitic magmas and to an instable stratified layered magma reservoir. Replenishment of fresh, hot primitive basaltic melts from the mantle provided enough heat and led to partial melting of amphibole-rich cumulates, generating water-rich hybrid basaltic to andesitic melts, and therefore triggering the turnover of this layered instable system with subsequent eruptions.

Petrographic, mineralogical and chemical criteria were used to demonstrate magma mixing of basaltic and andesitic to dacitic melts in the Akrotiri Volcanic Complex. Mixing must have occurred in a way such that primitive olivine basaltic melts, similar in composition to that of Cape Balos, were injected into a reservoir still filled to some extent with andesitic to dacitic melts. The fact that basaltic andesites of Cape Mavrorachidi are relatively homogeneous and that the groundmass consists of typical olivine basalt mineral composition (An_{74-68} and forsteritic olivine), indicates a lag time between onset of the mixing process and eruption.

7.3. ERUPTION MECHANISMS

Eruption mechanisms are dependent on magmatic processes in magma reservoirs as well as on their size and position at different crustal levels. In the Aegean island arc a major difference in the eruption mechanism seems to exist. The younger "Main Volcanic Series" of the Santorini islands as well as the most recent volcanics of Milos, Kos, Yali, and Nisyros are highly evolved rhyodacites and rhyolites, which erupted violently forming large pyroclastic deposits. The "Plinian-type" eruptions were followed by caldera collapses, which indicate large mass deficiencies at rather shallow crustal environments of a few kilometres depth. According to phenocryst assemblages and the absence of amphibole in the volcanic products, those magmas were subjected to low-pressure fractionation prior to eruption. As a consequence, hydrothermal systems could develop, which is demonstrated by hydrothermally altered volcanic products and fumarolic activity today. "Late stage volcanism" (eruptions after the major

volcanic climax) can lead to the final discharge of the largely degassed remaining magma chambers. The Kameni lavas in the Santorini caldera (Fig. 1), which were erupted between 197 B.C. and 1950 seem to demonstrate such a mechanism. The fact, that the low-temperature fumarolic activity and the low-enthalpy hydrothermal waters do not show any chemical changes during the last decades, indicates no recent magmatic replenishment of the reservoir.

In contrast, the volcanic islands of the western sector of the Aegean arc (Aegina, Methana, Poros) as well as the Akrotiri Volcanic Complex of the Santorini islands lack large quantities of pyroclastic rocks and caldera structures. Amphibole and biotite are the dominant hydrous phases present in all volcanic products.

The fact that large amounts of amphibole-rich basic inclusions and amphibole xenocrysts have been reported from the Columbos volcano by VOUGIOUKALAKIS and FRANCALANCI (1996) and by VOUGIOUKALAKIS et al. (1996) indicates magmatic processes similar to those discussed for the Akrotiri volcanic complex, e.g. discontinuous crystal fractionation and magma mixing.

Amphibole and biotite bearing andesitic to dacitic magmas, which are not subjected to low-pressure fractionation, must be derived from deeper crustal levels. These magmas do not seem to announce their ascent with long term (several months) magmatic precursors. Such rather rapid eruption mechanisms have been described in the 200 B.C. eruption of the Methana Kameni Chora andesite volcano and in the 1649/50 Columbos eruption northeast of Santorini. This latter most hazardous and largest historical eruption in the Aegean arc started on the seafloor in 300 m depth after a short time of seismic unrest in the spring of 1649 and finished after emission of approx. 2 km^3 of lavas and pyroclastics end of September 1650. A similar situation is indicated today between the Nisyros and Yali volcanic islands.

Replenishment of hot basaltic melt into cooling reservoirs at great crustal depth can partially remelt cumulates, trigger a turnover of a layered differentiated magma chamber and lead to ascent of the magmas.

Degassing of magmas, although not discussed within this paper, is a continuos process present in all magmas. In subduction related environments magmatic fluids and gases, such as H_2O, CO, CO_2, CH_4, SO_2, H_2, H_2S, N_2 etc. contribute to all magmatic processes. In the lavas the fluids are mainly concentrated in hydrous phases as amphibole and biotite.

The combination of noble gas ratios $^3He/^4He$, $^{20}Ne/^{22}Ne$ and $^{40}Ar/^{36}Ar$ compared to stable isotope ratios of C, H and O allows an appropriate discussion on the mantle and magmatic origin of the noble gases, the amount of atmospheric, meteoric and hydrothermal contamination, as well as the determination of equilibrium temperatures in the hydrothermal systems. It is known, that the noble gases are more sensitive and precise as indicators of changes of the magmatic regime (e.g. replenishment of new melts into magma reservoirs or emplacement of magmas from deep crustal levels to the surface) or changes of major tectonic processes (e.g. rapid extensional movements or crustal displacements). The $^3He/^4He$ ratios reflect well the high amount of mantle derived primordial ^3He in the Nisyros and Santorini fumarolic condensates as well as in some geothermal waters from Milos (DIETRICH et al., 1998). These results suggest that for the island of Nisyros, mantle-derived helium may be related to degassing of magmas, probably located at great crustal depth close to the mantle/crust boundary.

In order to detect such a deep seated magmatic process and to predict a new eruptive phase it is necessary to locate the size and depth of such a magma reservoir. This can be achieved by detailed seismic profiling and tomographic evaluation as well as by chemical and isotopic monitoring of fumarolic gases and hydrothermal waters.

Acknowledgements

This work was part of a three year programme on European Laboratory Volcanoes, Santorini, Greece and was financially sponsored by the European Commission, Directorate General for Science Research and Development DGXII - Environmental Programme and by the European Science Foundation Volcanology Programme (EVOP). We wish to thank C. Moor from the EMPA Dübendorf for carrying out the ICP-MS analyses. Ms. C. Büchel, Ms. D. Reber and T. Widmer, who kindly provided help with the manuscript and figures. Finally we are grateful to the Greek fishermen from Akrotiri who managed it perfectly to bring us with their little boats to very exposed and inaccessible cliffs in order to collect all the rock samples.

References

ALLEN, J.C., BOETCHER, A.L. and MARLAND, G. (1975): Amphiboles in andesites and basalt. I – Stability as a function of p-t-fO_2. Amer. Miner., 60, 1069–1085.

ALLEN, J.C., BOETCHER, A.L. (1978): Amphiboles in andesites and basalt. II – Stability as a function of P-T-fH_2O-fO_2. Amer. Miner., 63, 1074–1087.

BACON, CH.R. (1986): Magmatic inclusions in silicic and intermediate volcanic rocks. J. Geophys. Res., 91, 6091–6112.

BARTON, M. and HUIJSMANS, J.P.P. (1986): Post-caldera

dacites from the Santorini volcanic complex, Aegean Sea, Greece: an example of the eruption of lavas of near-constant composition over a 2,200 year period. Contrib. Mineral. Petrol., 94, 472–495.

BRIQUEU, L., JAVOY, M., LANCELOT, J.R. and TATSUMOTO, M. (1986): Isotope geochemistry of recent magmatism in the Aegean arc: Sr, Nd, Hf, and O isotopic ratios in the lavas of Milos and Santorini – geodynamic implications. Earth Planet. Sci. Lett., 80, 41–54.

DAVIS, E., GARTZOS, E. and DIETRICH, V.J. (1996): Magmatic evolution of the Pleistocene Akrotiri volcanoes. The European laboratory volcanoes. Second workshop Santorini, 2 to 4 May 1996, Abstract.

DIETRICH, V.J. (1989): Intramagmatic Pillowing. Terra, Vol. 1, No. 1, p. 278. Abstract.

DIETRICH, V.J., CARMAN, M.F., WYTTENBACH, A. and MCKEE, E.H. (1984): Geochemistry of basalts from Holes 519A, 520, 522 B and 524, Deep Sea Drilling Project Leg 73 (South Atlantic). Init. Rep. DSDP Vol. 73, 579–601.

DIETRICH, V.J., DAVIS, E. and GARTZOS, E. (1996): Amphiboles in rhyodacites and dacites from the Akrotiri volcanoes and the complexity of discontinous fractionation. The European laboratory volcanoes. Second workshop Santorini, 2 to 4 May 1996, Abstract.

DIETRICH, V.J., GAITANAKIS, P., MERCOLLI, I. and OBERHÄNSLI, R. (1994): Geological Map of Greece – Aegina Island 1:25'000. Bull. Geol. Soc. Greece. Vol. XXVIII/3, 555–566.

DIETRICH, V.J., HURNI, L. and GAITANAKIS, P. (1995): Geological Map of Greece. Methana (Saronic Gulf), 1 : 25'000 with explanations. Stiftung Vulkaninstitut Immanuel Friedlaender, Zürich. Verlag Birkhäuser, Basel and IGME (Athen).

DIETRICH, V. J., KIPFER, R. and SCHWANDNER, F. (1998): Mantle-derived noble gases in the South Aegean volcanic arc: Indicators for incipient magmatic activity and deep crustal movements. Newsletter of the European Centre on Prevention and Forecasting of Earthquakes (Council of Europe, Sept. 1998), 28–32.

DIETRICH, V.J., MERCOLLI, I. and OBERHÄNSLI, R. (1988): Dazite, High-Alumina-Basalte und Andesite als Produkte Amphibol-dominierter Differentiation (Aegina und Methana, Aegäischer Inselbogen). Schweiz. Mineral. Petrogr. Mitt., 68, 21–39.

DIETRICH, V.J., MERCOLLI, I. and OBERHÄNSLI, R. (1987): The complexity of discontinuous fractionation in water-bearing magmas. Program IAVCEI, V.3–P3, p. 407.

DRUITT, T.H. (1985): Vent evolution and lag breccia formation during the Cape Riva eruption of Santorini, Greece. J. Geol., 93, 439–454.

DRUITT, T.H. (1996): Volcanic evolution of Santorini. Exkursion guide. 2nd workshop on European Laboratory Volcanoes, Santorini, Greece, May 2–4, 1996.

DRUITT, T.H., L. EDWARDS, L., LANPHERE, M., SPARKS, R.S.J. and DAVIS, M. (1998): Volcanic development of Santorini revealed by field, radiometric, chemical and isotopic studies. In CASALE, R., FYTIKAS, M., SIGVALDASSON, G. and VOUGIOKALAKIS, G. (eds): The European laboratory volcanoes, European Commission EUR 18161 en, 37–47.

DRUITT, T.H. and FRANCAVIGLIA, V. (1992): Caldera formation on Santorini and the physiography of the islands in the late Bronze Age. Bull. Volcanol., 54, 484–493.

DRUITT, T.H., MELLORS, R.A., PYLE, D.M. and SPARKS, R.S.J. (1989): Explosive volcanism on Santorini, Greece. Geol. Mag., 126, 95–126.

EICHELBERGER, J.C. (1980): Vesiculation of mafic magma during replenishment of silicic magma reservoirs. Nature, 288, 446–450.

EICHELBERGER, J.C. (1975): Origin of andesite and dacite: evidence of mixing at Glass Mountain in California and other circum-Pacific volcanoes. Geological Society of America Bulletin 86, 1381–1891.

EVENSEN, N.M., HAMILTON, P.J. and O'NIONS, R.K. (1978): Rare earth abundances in chondritic meteorites. Geochim. Cosmochim. Acta, 42, 1199–1212.

FEELEY T.C. and DUNGAN, M.A. (1996): Compositional and dynamic controls on mafic-silicic magma interactions at continental arc volcanoes: evidence from Cordón el Guadal, Tatara-San Pedro complex, Chile. J. Petrology, 37, 1547–1577.

FOUQUE, F. (1879): Santorin et ses éruptions. Masson et Cie, Paris.

FYTIKAS, M., GUILIANI, O., INNOCENTI, F., MARINELLI, G. and MAZZUOLI, R. (1976): Geochronological data on recent magmatism of the Aegean Sea. Tectonophysics, 31, 29–34.

FYTIKAS, M., INNOCENTI, F., KOLIOS, N. MANETTI, P., MAZZUOLI, R., POLI, G., RITA, F. and VILLARI, L. (1986): Volcanology and Petrology of Volcanic Products from the Island of Milos and Neighbouring Islets. J. Volcanol. Geotherm. Res., 28, 297–317.

FYTIKAS, M., INNOCENTI, F., MANETTI, P., MAZUOLI, R., PECCERILO, A. and VILLARI, L. (1984): Tertiary to Quaternary evolution of the volcanism in the Aegean Region. In: DIXON, J.E. and ROBERTSON, A.H.F. (eds): The Geological Evolution of the Eastern Mediterranean. Geol. Soc. London. Spec. Pub. 17, 687–699.

FYTIKAS, M., KOLIOS, N. and VOUGIOUKALAKIS, G. (1990): Post-Minoan volcanic activity of the Santorini volcanoe. Volcanic hazard and risk. Forecasting possibilities. In: Thera and the Aegean World III, 2, 183–198. The Thera Foundation, London.

GARTZOS, E., DIETRICH, V.J. and DAVIS, E. (1998): Magma mixing in basaltic andesites of Cape Mavrorachidi (Akrotiri volcanoes). The European laboratory volcanoes. Second workshop Santorini, 2 to 4 May 1996, Abstract.

GUELEN, L., HART, S.R., SALTERS, V.J.M., WYERS, G.P. and BARTON, M. (1987): Sr, Nd, Pb, isotopic constraints on the petrogenesis of the Aegean arc volcanics. Terra Cognita, 7, 170–171.

GUELEN, L. (1990): Isotopic characterization of Aegean magmatism and geodynamic evolution of the Aegean subduction. Internat. Earth Sci. Congr. On Aegean Regions, Oct. 1–6 (1990) Izmir/Turkey, Proceedings 2, 143–166.

HUIJSMANS, J.P.P (1985): Calcalkaline lavas from the volcanic complex of Santorini, Aegean Sea, Greece. A petrological, geochemical and stratigraphic study. Ph.D. thesis, Rijksuniversiteit Utrecht.

HUIJSMANS, J.P.P. and BARTON, M. (1983): Petrographic and geochemical evidence for the role of magma mixing and fractional crystallisation in zoned magma chambers on Santorini, Cyclades, Greece. I.U.G.G., XVIII General Assembly, IAVCEI, 1983, p. 67. Abstract.

HUIJSMANS, J.P.P., BARTON, M. and SALTERS, V.J.M. (1988): Geochemistry and evolution of the calc-alkaline volcanic complex of Santorini, Aegean Sea, Greece. J. Volcanol. Geotherm. Res., 34, 283–306.

KALOGEROPOULOS, S. and PARITSIS, S. (1990): Geological and Geochemical evolution of the Santorini volcano: a review, In: Thera and the Aegean World III, 2, 164–171. The Thera Foundation, London.

KOYAGUCHI, T. (1986): Textural and compositional evidence for magma mixing and its mechanism, Abu

volcano group, southwestern Japan. Contrib. Mineral. and Petrol., 93, 33–45.

LEAKE, B.E. (1978): Nomenclature of amphiboles. Amer. Mineral., 63,1023–1052.

MANN, A.C. (1983): Trace element geochemistry of high alumina basalt – andesite – dacite – rhyodacite lavas of the main volcanic series of Santorini volcano, Greece. Contrib. Mineral. Petrol., 84, 43–57.

MCBIRNEY, A.R. (1980): Mixing and unmixing of magmas. J. Volcanol. Geotherm. Res., 7, 357–371.

MERCOLLI, I., DIETRICH, V. and OBERHÄNSLI, R. (1989): Origin of Dacites by Magma Mingling. Terra, Vol. 1, No. 1, p. 278. Abstract.

MITROPOULOS, P. and TARNEY, J. (1992): Significance of mineral composition variations in the Aegean Island Arc. J. Volcanol. Geotherm. Res., 51, 283–303.

MITROPOULOS, P., TARNEY, J., SAUNDERS, A.D. and MARSH, N.G. (1987): Petrogenesis of Cenozoic Volcanic Rocks from the Aegean Island Arc. J. Volcanol. Geotherm. Res. 32, 177–193.

NICHOLLS, I.A. (1971): Petrology of Santorini Volcano, Cyclades, Greece. J. Petrology, 12, Part 1, 67–119.

NICHOLLS, I.A. (1978): Primary basaltic magmas for the pre-Caldera volcanic rocks of Santorini. In DOUMAS, C. (ed.): Thera and the Aegean World I, 109–120.

NISBET, E.G., DIETRICH, V.J. and ESENWEIN, A. (1979): Routine trace element determination in silicate minerals and rocks by X-ray fluorescence. Fortschr. Mineral. 57/2, 264–279.

OBERHÄNSLI, R., MERCOLLI, I. and DIETRICH, V.J. (1985): The amphibole-andesite connection. Terra cognita, 5, 2/3, 213.

OBERHÄNSLI, R., DIETRICH, V. and MERCOLLI, I. (1989): Origin of High-Alumina Basalts by Hybridisation of Cumulates. Terra, 1, p. 277. Abstract.

OSBORN, E.F. and RAWSON, S.A. (1980): Experimental studies of magnetite in calc-alkaline rocks. Carnegie Inst. Washington, Yearbook, 79, 281–285.

OSBORN, E.F. (1976): Origin of calc-alkali magma series of Santorini volcano type in the light of recent experiments phase equilibria. In: Proc. Int. Cong. Therm. Waters, Geotherm. Energy, Volcanism, Med. Area, 1976, Vol. 3, 154–167.

PAPAZACHOS, C., KIRATZI, A. and PAPAZACHOS, B. (1992): Rates of active crustal deformation and its application to central Greece. Geophys. J. Int., 111, 424–432.

PAPAZACHOS, B. and PANAGIOTOPOULOS, D. (1993): Normal faults associated with volcanic activity and deep rupture zones in the southern Aegean volcanic arc. Tectonophysics, 220, 301–308.

PEARCE, J.A. (1982): Trace element characteristics of lavas from destructive plate boundaries. In THORPE, R.S. (ed.): Andesites, 525–548.

PECCERILLO, A. and TAYLOR, S.R. (1976): Geochemistry of Eocene calkalkaline volcanic rocks from Kastamonu Area, Northern Turkey. Contr. Mineral. Petrol., 58, 63–81.

PERISSORATIS, C., ZACHARAKIS, P., MICHAILIDIS, S. and ZIMIANITIS, E. (1995): Surficial Sediment Map of the Aegean Sea Floor. Santorini (Thira) Sheet 1 : 200'000. IGME, Athens.

PICHLER, H. and KUSSMAUL, S. (1980): Comments on the geological map of the Santorini islands Thera and the Aegean World II. In: Thera and the Aegean World II, 413-427. The Thera Foundation, London.

SAUNDERS, A.D. and TARNEY, J. (1984): Geochemical characteristics of basaltic volcanism within back-arc basins. In: KOKELAAR, B.P. and HOWELLS, M.F. (eds): Marginal basin geology. Spec. Publ. Geol. Soc. London, 16, 59–76.

SCHMIDT, M.W. (1992): Phase compositions and relationships in tonalite: an experimental approach. Ph.D. Thesis ETH Zurich, No. 9897, 113 pp.

SEIDENKRANTZ, M.S. and FRIEDRICH, W.L. (1986): Santorini, Part of the Hellenic Arc: Age relationship of its earliest volcanism. In: SEIDENKRANTZ, M.S.: Foraminiferal analyses of shelf areas. Stratigraphy, Ecology and Taxonomy. Ph. D. Thesis, University of Aarhus, 41–65.

SEMET, M.P. and ERNST, W.G. (1981): Experimental stability relations of magnesio hastingsite. Geol. Soc. Amer. Bull. 92, 71–74.

SEWARD, D., WAGNER, G.A. and PICHLER, H. (1980): Fission track ages of Santorini volcanics. In: Thera and the Aegean World II, 101–108. The Thera Foundation, London.

SISSON, T.W. and GROVE, T.L. (1993): Experimental investigations of the role of H_2O in calc-alkaline differentiation and subduction zone magmatism. Contrib. Mineral. Petrol., 113, 143–166.

SISSON, T.W. and GROVE, T.L. (1993): Temperatures and H_2O contents of low-MgO high-aluminia basalts. Contrib. Mineral. Petrol., 113, 167–184.

SUN, S.S., NESBITT, R.W. and SHARASKIN, A.Y. (1979): Geochemical characteristics of mid-ocean ridge basalts. Earth Planet. Sci. Lett., 44, 119–138.

THORNTON, C.P. and TUTTLE, O.F. (1960): Chemistry of igneous rocks; pt. I. Differentation Index. Amer. J. Sci., 258, 664–684.

ULMER, P. and TROMMSDORFF, V. (1995): Serpentine stability to mantle depths and subduction-related magmatism. Science 268, 858–861.

VOUGIOUKALAKIS, G. and FRANCALANCI, L. (1996): Post-Minoan activity. Exkursion guide. 2nd workshop on European Laboratory Volcanoes, Santorini, Greece, May 2–4, 1996.

VOUGIOUKALAKIS, G., FRANCALANCI, L., MITROPOULOS, D. and PERISSORATIS, K. (1996): The 1649–1650 eruption of the Kolumbo submarine volcanic centre, Santorini. Abstracts of the 2nd workshop on European Laboratory Volcanoes, Santorini, Greece, May 2–4, 1996.

WRIGHT, T.L. and DOHERTY, P.C. (1970): A linear programming and least squares Computer method for solving petrologic mixing problems. Geol. Soc. Amer. Bull., 81, 1995–2008.

WYERS, G.P. and BARTON, M. (1989): Polybaric evolution of calc-alkaline magmas from Nisiros, southeastern Hellenic arc, Greece. J. Petrol., 30, 1–37.

WYERS, G.P., BARTON, M. and FOLAND, K.A. (1987): Sr- and Nd-isotopic evidence for magma mixing and assimilation in two shield volcanoes on Santorini, Aegean Sea, Greece. Geol. Soc. Amer. Abstracts., Prog. 19, 900.

Manuscript received June 23, 1997; revision accepted April 25, 1999.

Appendix

SAMPLE LOCALITIES

Cape Balos high-alumina olivine basalt (bulk chemistry in Tab. A1)

Bal 8:

Cape Balos (lower most pyroclastic layer, basaltic scoria).

Bal 10:

Cape Balos (basaltic scoria, base of plug). Mineralogy same as Bal 8.

Bal 12:

Cape Balos Chapel (basaltic scoria, base of flow).

Bal 15:

Cape Balos Plug (internal part). Basalt; mineralogy same as Bal 12.

Kok 2:

Cape Kokkinopetra (bomb from scoria). Basalt; mineralogy: plagioclase, clinopyroxene, and orthopyroxene; similar as Balos basalt.

Cape Mavrorachidi high-Mg basaltic andesite (bulk chemistry in Tab. A1)

Rdch2:

Cape Mavrorachidi (bomb from scoria). Basaltic andesite with magma mixing phenomena. Mineralogy same as Cmav2 and 3.

Cmav2:

Cape Mavrorachidi (base of lava flow behind chapel). Basaltic andesite with magma mixing phenomena.

Cmav3:

Cape Mavrorachidi (front of lava flow). Basaltic andesite.

Basaltic andesites and andesites (bulk chemistry in Tab. A1)

Messa 2:

E of Mt. Arkhangelos (altered basaltic andesite dike). Porphyritic texture. Mineralogy: plagioclase, clinopyroxene (partly corroded and as clusters), opaques.

Messa 8:

SW of Mt. Loumaravi (altered basaltic andesite dike). Porphyritic texture. Abundant quartz oicelli with clinopyroxenitic reaction rims. Mineralogy: plagioclase, clinopyroxene, Ti-magnetite. Xenocrysts: Plagioclase, decomposed opacitic amphibole.

Arhan 7:

SE of Mt. Arkhangelos road (altered basaltic andesite dike). Texture and mineralogy similar to Messa 8.

Arhan 2:

E slope Mt. Arkhangelos (altered dolerite component in epiclastic flows). Intersertal texture. Mineralogy: plagioclase, calcite and chlorite (pseudomorph after clinopyroxene), Ti-magnetite.

Cakro 21:

SE Cape Arkrotiri, sea level (Andesite components in lowermost 23 and 24 pumice rich epiclastics). Mineralogy: plagioclase, clinopyroxene, hypersthene, opaques, and glass.

Cakro 33:

Cape Akrotiri, E of lighthouse (andesitic components in pumice-rich 34 and 36b epiclastics above beach conglomerate). Glass rich, porous, vitrophyric andesites. Mineralogy: phenocrysts of plagioclase, clinopyroxene and orthopyroxene. Xenocrysts: anorthitic plagioclase, olivine rimmed by clinopyroxene, clinopyroxene and pseudomorphic aggregates of clinopyroxene; opaques, clinopyroxene and glass aggregates pseudomorph after amphibole. Magma mixing phenomena.

Kast 6a:

Foothill of Castello (village of Akrotiri). Same textures and mineralogy as in Cakro 33–36.

Kast 2:

S of village of Akrotiri (black andesitic dacite component in rhyodacitic pumice). Same textures and mineralogy as in Cakro 33–36.

Andesitic dacites and dacites (bulk chemistry in Tab. A2)

WHB 3:

Cliff at sealevel, SW of Mt. Arkhangelos (dacitic sill in hydrothermally altered epiclastics).

Cvun 7:

E of Cape Vounia, sea level (andesite). Porphyritic and glomeroporphyritic textures; rich in plagioclase-clinopyroxene clusters. Xenocrysts: plagioclase.

Cvun 9:

W of Cape Vounia at sea level (andesite plug and pyroclastics equivalent to monolithos or obelisk). Mineralogy similar as Cvun 7.

Cvun 1:

E of Cape Vounia, sea level. Dacitic component in rhyodacitic pyroclastics.

Cvun 2:

E of Cape Vounia, sea level. Andesitic component in rhyodacitic pyroclastics. Mineralogy same as Cvun 1.

Mavro 1:

W part of Cape Mavros, sea level (lowermost

hyaloclastic dacitic part). Mineralogy same as in Mavro 2.

Mavro 2:

W part of Cape Mavros: (andesitic to dacitic plug, main phase). Porphyritic and glomeroporphyritic textures; rich in plagioclase-clinopyroxene clusters. Xenocrysts: plagioclase.

Mavro 5:

E part of Cape Mavros, sea level. Mineralogy same as in Mavro 2.

Mavro 6:

E part of Cape Mavros, sea level (dacite). Texture and mineralogy similar to Mavro 2.

Mavro 4:

E part of Cape Mavros, sea level (dacite). Glass rich variety of Mavro 5.

Cvun 1a:

E of Cape Vounia, sea level. High-Ti andesite as component in rhyodacitic pyroclastics.

Arhan 9:

S of Mt. Arkhangelos (100 m altitude). Relict of small cinder cone. Welded scoria. High-Ti andesite.

Rhodacitic lavas (bulk chemistry in Tab. A2)

Bal 3:

E of Cape Balos (white rhyodacite component in lowermost pumice rich rhyodacitic pyroclastic flows.

Rdch 1:

Beach W of Cape Mavroachidi (white rhyodacite component in pumice rich epiclastic flows).

Akro 1:

Rhyodacite flow S of village of Akrotiri. Glassy matrix. Mineralogy very similar to Rdch 1.

Cakro 1:

Cape Akrotiri (rhyodacitic flow, glassy matrix).

Cakro 17:

SE Cape Akrotiri, sea level (pumice component from base of rhyodacitic Akrotiri flows). Mineralogy similar as Cakro 1.

Cakro 20:

SE Cape Akrotiri, sea level (glass rich pyroclastic base of rhyodacitic Akrotiri flows). Mineralogy similar as Cakro 1.

Cakro 36a:

Cape Akrotiri, E of Lighthouse (dacitic component in pumice rich epiclastics above beach conglomerate). Rhyodacitic groundmass (containing green magnesio hornblende) with numerous small (1–3 mm in diametre) dacitic inclusions (Type Cakro 33 and 34) and plagioclase xenocrysts.

Cvun 3:

E of Cape Vounia, sea level (dacitic component from oldest rhyodacitic pyroclastics). Texture and Mineralogy very similar to Cakro 36a).

Basic Inclusions in Rhyodacite: Cape Akrotiri (bulk chemistry in Tab. A3)

Cakro 3:

Amphibole-plagioclase inclusion. Texture: fine-grained acicular, porous. Plagioclase and greenish amphibole, traces of clinopyroxene. Compositions very similar to Cakro 12.

Cakro 4:

Basaltic inclusion similar in texture and mineralogy to Cakro 5.

Cakro 7:

Amphibole-plagioclase inclusion. Texture: medium-grained (amphibole up to 5 mm), acicular, porous. Mineralogy: plagioclase, clinopyroxene, coarse brownish amphibole (magnesio-hastingsite), Ti-magnetite, glass.

Cakro 8:

Amphibole-plagioclase inclusion. Texture and mineralogy similar to Cakro 7.

Cakro 10:

Amphibole-plagioclase inclusion. Texture coarse-grained acicular, very porous. Mineralogy similar to Cakro 11.

Cakro 11:

Amphibole-plagioclase inclusion. Texture: coarse-grained (amphibole up to 1 cm), acicular, porous. Mineralogy: plagioclase An_{86-81} (centres), An_{69-61} (intermediate), An_{46-44} (rims); amphibole (magnesio-hastingsite, high in Al_2O_3 (up to 14 wt%), Ti-magnetite, rhyolitic glass.

Cakro 12:

Amphibole-plagioclase inclusion. Texture: medium-grained, acicular, porous. Mineralogy: plagioclase An_{77-62}, magnesio-hastingsitic amphibole, orthopyroxene $En_{58-55;}$ rhyolitic glass (SiO_2 up to 84 wt%), Ti-magnetite, interstitial glass partly of anorthoclase/alkalifeldspar composition.

Cakro 6:

Amphibole-plagioclase inclusion. Texture: fine-grained, acicular, porous. Mineralogy similar to Cakro 3: plagioclase, clinopyroxene rimmed by amphibole. Ti-magnetite, glass.

Cakro 9:

Glass-rich amphibole-plagioclase inclusion. Mineralogy: plagioclase, glass, clinopyroxene-Ti-magnetite aggregates, large amphiboles (magnesio-hastingsite).

Cakro 25:

SE of Cape Akrotiri, sea level. Basaltic components in lowermost pumice-rich and 26: rhyodacitic epiclastic flows.

Cakro 5:

Basaltic component. Texture: fine-grained vesicular and very porous. Mineralogy: plagio-

clase An_{75-60}, clinopyroxene rimmed by magnesiohastingsitic amphibole; Ti-magnetite.

Rhyolites (components and pumice in lowermost Akrotiri pyroclastics, e.g. Cakro 19)

Cakro 18

SE Cape Akrotiri, sea level (red rhyolitic components in lowermost and 19 pumice rich epiclastic flows).

Bal 9:

Cape Balos (rhyolitic xenolith in lowermost Balos scoria). Mineralogy similar as Cakro 18 and 19.

ANALYTICAL TECHNIQUES

Mineral chemistry

A Cameca SX50 microprobe with 5 crystal spectrometers was used for the analyses. To minimise the excitation volume the beam was set to 12 kV and 20 nA. A slightly defocused electron beam was used to prevent the beam from affecting the sample during the total counting time of 96 seconds. Eleven elements were measured with variable peak counting times of 10 sec (Si, Al, Ca, Mg, Na, K), 24 sec (Fe, Mn, Ti, Cr, Ni). Data were processed with PAP-correction, which is a modified ZAF correction procedure.

Amphibole compositions were normalised by assuming (i) fixed $Fe^{3+}/(Fe^{3+} + Fe^{2+})$ ratio of 0.2 and 23 oxygens, and (ii) cations – Ca–Na–K = 13. Clinopyroxenes were normalised with a slightly modified scheme, obtaining cation-sums from 3.97 to 4.04, a deviation from the "ideal" value of 4.00 which lies within the range of instrumental errors of microprobe analyses.

Bulk rock chemistry

Major-element bulk chemical composition was determined by the X-ray fluorescence (XRF) analysis (Tabs A1 to A3) of glass beads; the glass beads were fused from ignited powders plus $Li_2B_4O_7$ ($^1/_5$ ratio) in a gold-platinum dish at 1150 °C (DIETRICH et al., 1984). The XRF analyses were performed with an automated Philips sequential spectrometer (PW 1404) at the Eidgenössische Materialprüfungsanstalt, EMPA, Dübendorf, Switzerland. The data were corrected for drift, background, and matrix effects. Twelve USGS reference rock samples were used for calibration. FeO content was determined colorimetrically. Nb, Zr, Y, Sr, U, Rb, Th, Pb, Ga, Zn, Cu, Ni, Co, Cr, V, Ce, Nd, Ba, La, Sc, and S trace-element abundances were also analysed by using X-ray fluorescence; 10-g powder samples were analysed by using the synthetic background method, in which major-element contents are known. A computer program was used to calculate background, interference, and mass absorption effects as well as standard deviations (NISBET et al., 1979). The USGS reference samples were used for calibration. The resulting accuracy was ± 10 to 20% at 10 ppm. A chromium tube was used; detection limits were around 3 to 5 ppm for most trace elements.

The trace elements Nb, Be, Li, Hf, Ta, Th, and U (Tabs A1 to A3) as well as the Rare Earth Elements were analysed from sample solutions using an inductively coupled plasma mass spectrometer (ICP-MS) ELAN 5000 (Perkin-Elmer, Sciex) at the EMPA, Dübendorf, Switzerland, calibrated with pure standard solutions; detection limits approx. 1–10 ppb.

Tab. A1 Bulk chemical compositions of basalts, basaltic andesites and andesites from Akrotiri volcanoes.

wt%	Bal 12	Bal 15	Kok 2	Rdch 2	Cmav 2	Messa 2	Messa 8	Cakro 21	Cakro 23	Cakro 24	Cakro 33	Cakro 34
SiO_2	49.93	49.23	50.88	53.08	53.25	54.09	54.95	57.17	58.98	55.5	57.11	58.02
TiO_2	0.85	0.85	0.86	0.8	0.8	1.01	0.73	0.91	0.82	1.01	0.61	0.59
Al_2O_3	18.02	17.41	17.75	15.87	15.81	16.17	17.67	16.99	17.34	17.66	16.94	16.68
Fe_2O_3	7.72	6.14	8.97	1.01	1.78	2.16	6.83	2.83	2.98	0.82	6.01	6.13
FeO	1.15	2.55	0.3	6.6	5.87	6.05	0.45	4.4	1.97	5.4	0.45	0.35
MnO	0.16	0.15	0.16	0.14	0.15	0.17	0.12	0.15	0.09	0.13	0.13	0.13
MgO	6.14	7.48	7.29	7.52	7.35	5.35	4.95	3.58	2.68	3.57	4.49	4.57
CaO	11.55	11.07	10.78	9.16	9	9.18	9.7	7.48	7.02	8.53	8.62	8.37
Na_2O	2.64	3.89	1.71	3.28	3.77	3.52	2.58	3.74	4.36	3.64	2.65	2.62
K_2O	0.36	0.47	0.45	1.16	1.3	1.12	0.69	1.15	1.44	1.19	1.07	1.09
P_2O_5	0.09	0.12	0.13	0.12	0.13	0.16	0.11	0.17	0.15	0.14	0.09	0.09
H_2O^+	0.52	0.61	0.5	0.97	0.61	0.93	1.48	1.59	1.89	2.01	1.28	1.1
Total	99.15	99.99	99.81	99.77	99.87	99.93	100.27	100.16	99.72	99.6	99.46	99.77
D.I.	28.4	34.3	25.6	34.6	39.6	39.1	38.1	49.7	57.1	43.7	43.8	45
Nb	4	4	< 3	7	6	7	< 3	7	8	7	5	< 3
Be	0.45	0.38	0.44	0.69	0.79	0.77	0.58	1.06	1.05	0.9	0.5	0.63
Zr	52	53	74	112	114	128	87	133	115	99	97	105
Y	13	11	12	13	13	21	16	18	11	16	9	9
Sr	212	211	268	150	150	185	321	224	222	236	184	184
Ba	88	91	155	187	199	182	326	317	316	284	190	199
Rb	8	10	10	28	30	26	23	25	31	26	22	21
Li	4.54	3.19	2.92	8.31	5.25	7.85	5.14	3.9	5.57	3.49	7.76	10.2
Hf	1.71	1.66	2.13	2.91	3.39	3.79	2.54	3.54	3.32	3.12	2.88	3.05
Ta	0.13	0.25	0.1	0.53	0.59	0.3	0.3	0.58	0.53	0.44	0.16	0.18
Th	1.1	1.23	0.9	5	6.5	5.5	5.4	6.2	8.17	5.99	4.11	4.64
U	0.29	0.11	0.49	1.79	1.88	1.98	1.85	2.11	3.64	2.55	1.13	1.25
Ga	12	12	12	11	13	12	12	13	11	13	10	11
Zn	56	59	60	66	60	70	55	74	61	81	56	54
Cu	41	34	20	54	49	28	55	8	< 3	15	4	9
Co	28	38	21	27	149	17	7	5	< 3	< 3	< 3	< 3
V	259	224	234	231	197	215	247	242	145	250	178	162
Ni	52	64	73	101	96	39	26	< 3	12	14	25	32
Cr	142	128	223	309	268	135	51	4	20	20	62	147
Sc	36	33	34	34	30	32	26	26	16	28	22	22
F	< 30	< 30	< 30	235	138	142	412	165	258	198	< 30	< 30
La	6.97	6.17	9.35	12.9	17.5	14	17.1	19.8	21.2	16.7	11.9	13.9
Ce	15	14.1	21	28	32.5	30.3	32.8	37.8	40	32.9	22.5	24.8
Pr	2.23	1.96	2.79	3.07	3.91	3.86	4.37	4.36	4.4	3.83	2.84	3.14
Nd	10.8	8.91	11.7	12.3	15.9	16.7	17.7	17.3	17.3	15.7	10.9	11.9
Sm	3.19	2.55	2.8	2.92	3.75	4.62	3.78	4.04	4.14	4.12	2.29	2.48
Eu	1	0.83	0.98	0.69	0.96	1.29	1.12	1.14	1.28	1.32	0.8	0.85
Gd	3.7	3.5	3.32	3.24	4.34	5.5	4.2	4.4	4.57	4.85	2.6	2.78
Tb	0.58	0.51	0.55	0.47	0.6	0.86	0.67	0.65	0.63	0.62	0.45	0.45
Dy	3.65	3.34	3.54	3.1	3.91	4.87	4.18	4.34	4.2	4.37	3.13	3.13
Ho	0.78	0.72	0.76	0.68	0.87	1.04	0.89	0.93	0.87	0.94	0.7	0.69
Er	2.39	2.04	2.2	1.97	2.57	3.26	2.46	2.7	2.65	2.88	1.95	2.1
Tm	0.35	0.32	0.33	0.29	0.39	0.47	0.4	0.42	0.4	0.41	0.32	0.32
Yb	2.3	2	2.06	1.92	2.35	2.85	2.48	2.48	2.37	2.72	2.05	2.02
Lu	0.32	0.29	0.31	0.27	0.36	0.44	0.37	0.39	0.36	0.38	0.3	0.3

Tab. A2 Bulk chemical compositions of andesitic dacites, dacites and rhyodacites from Akrotiri volcanoes.

wt%	WHB 3	Cvun 9	Cvun 1	Mavro 1	Mavro 4	Cvun 1a	Cakro 18	Bal 3	Rdch 1	Akro 1	Cakro 1	Cakr 36a
SiO_2	59.71	58.90	57.75	59.99	61.07	57.80	71.12	68.49	66.47	67.42	67.52	63.50
TiO_2	0.76	0.80	0.81	0.83	0.69	1.21	0.37	0.39	0.43	0.43	0.39	0.55
Al_2O_3	16.31	16.79	16.81	16.17	15.81	15.70	14.03	14.50	14.50	14.44	14.44	16.10
Fe_2O_3	5.00	6.18	1.65	1.30	2.12	1.03	0.78	1.51	0.89	0.31	1.36	4.59
FeO	0.50	0.36	4.70	4.05	3.20	6.45	1.65	1.20	1.90	2.40	1.49	0.36
MnO	0.10	0.13	0.14	0.13	0.08	0.13	0.04	0.08	0.09	0.09	0.08	0.11
MgO	2.85	3.27	3.38	2.87	2.90	2.28	0.29	1.26	1.52	1.26	1.38	2.48
CaO	5.39	6.79	6.78	5.77	5.53	5.36	2.55	2.76	3.24	2.95	2.87	5.54
Na_2O	4.21	3.29	3.97	4.16	4.63	4.97	4.72	5.32	4.61	4.79	5.05	3.37
K_2O	1.66	1.64	1.65	1.96	2.11	2.48	2.49	2.28	2.71	2.77	2.58	1.86
P_2O_5	0.15	0.14	0.15	0.15	0.15	0.26	0.10	0.11	0.12	0.12	0.11	0.09
H_2O^+	2.68	1.55	1.93	2.38	1.54	2.13	1.32	2.01	3.39	2.97	2.63	0.97
Total	99.32	99.84	99.72	99.76	99.83	99.80	99.46	99.91	99.87	99.95	99.90	99.52
D.I.	60.00	53.40	51.80	58.20	62.80	60.30	82.80	80.50	75.40	77.30	78.80	61.80
Nb	4	3	8	n.d.	n.d.	17	10	10	12	10	10	7
Be	1.13	0.97	1.13	n.d.	n.d.	1.48	1.69	1.93	1.65	1.69	1.79	0.97
Zr	122	120	118	116	128	250	158	176	154	163	169	129
Y	12	17	15	18	17	30	5	14	10	15	11	13
Sr	198	213	244	212	199	155	173	188	237	209	184	203
Ba	278	377	417	375	377	383	595	563	535	551	581	545
Rb	29	55	49	42	32	76	59	61	53	83	61	50
Li	1.48	3.43	4.47	n.d.	n.d.	10.4	n.d.	n.d.	n.d.	n.d.	9.57	5.36
Hf	3.53	3.55	3.41	n.d.	n.d.	6.58	0.84	4.62	4.68	4.61	3.78	2.86
Ta	0.4	0.34	0.44	n.d.	n.d.	16.4	1.30	1.20	0.95	1.10	1.32	0.48
Th	2.9	3.22	7.54	n.d.	n.d.	11.97	8.20	16.10	16.30	10.00	14.70	11.40
U	4.4	3.46	2.95	n.d.	n.d.	4.26	1.75	6.10	5.59	5.28	6.20	3.70
Ga	11	13	12	13	12	15	8	9	8	10	10	10
Zn	39	51	54	54	50	85	16	30	32	33	33	40
Cu	6	11	11	< 3	7	26	< 3	< 3	< 3	< 3	< 3	< 3
Co	< 3	< 3	< 3	< 3	< 3	156	24	15	37	12	8	12
V	109	157	190	180	137	187	35	32	39	48	34	89
Ni	11	18	14	< 3	15	11	< 6	< 6	< 6	< 6	< 6	8
Cr	10	19	8	< 3	21	4	6	< 3	< 3	< 3	< 3	13
Sc	15	19	22	19	15	20	3	4	5	6	6	10
DF	339	45	184	243	300	512	189	123	48	105	111	< 30
La	7.60	10.70	21.50	23.10	n.d.	32.70	4.19	10.90	15.80	10.70	19.90	4.12
Ce	17.10	24.30	42.20	42.40	n.d.	67.90	9.50	23.30	31.20	21.10	37.10	9.18
Pr	2.12	2.84	4.55	4.72	n.d.	7.51	1.12	2.79	3.63	2.56	4.16	1.25
N.d.	8.42	11.40	17.80	18.30	n.d.	29.20	4.25	10.60	13.00	9.55	15.00	4.67
Sm	1.99	2.59	4.03	4.21	n.d.	6.73	1.00	2.23	2.72	2.21	3.30	1.20
Eu	0.71	0.86	1.27	1.15	n.d.	1.63	0.21	0.53	0.66	0.55	0.88	0.37
Gd	2.51	3.26	4.63	4.76	n.d.	7.58	1.01	2.18	2.91	2.34	3.10	1.25
Tb	0.44	0.58	0.75	0.68	n.d.	1.16	0.14	0.31	0.40	0.30	0.45	0.25
Dy	3.08	3.90	3.89	4.56	n.d.	6.78	0.87	2.34	2.75	2.32	2.84	1.86
Ho	0.70	0.80	0.83	1.01	n.d.	1.44	0.19	0.53	0.60	0.51	0.61	0.43
Er	2.18	2.30	2.62	2.93	n.d.	4.37	0.58	1.65	1.92	1.58	1.99	1.30
Tm	0.34	0.37	0.38	0.46	n.d.	0.64	0.10	0.28	0.31	0.27	0.31	0.23
Yb	2.16	2.28	2.48	2.68	n.d.	3.97	0.73	1.75	2.05	1.87	1.94	1.52
Lu	0.34	0.37	0.36	0.43	n.d.	0.60	0.13	0.29	0.33	0.29	0.32	0.23

Tab. A3 Bulk chemical compositions of basic inclusions in Cape Akrotiri rhyodacite.

wt%	Cakro 7	Cakro 11	Cakro 12	Cakro 9	Cakro 25	Cakro 5
SiO_2	50.44	49.33	51.75	54.74	50.32	50.27
TiO_2	1.06	1.09	1.06	0.90	0.92	0.82
Al_2O_3	18.08	19.04	18.00	17.83	17.80	18.12
Fe_2O_3	5.73	8.12	7.08	4.01	5.86	4.42
FeO	4.40	2.80	3.05	4.50	3.57	4.05
MnO	0.20	0.21	0.21	0.20	0.17	0.15
MgO	4.80	3.95	4.63	3.47	5.09	5.35
CaO	8.51	9.10	8.44	7.38	10.25	11.58
Na_2O	4.20	3.54	3.81	4.61	3.39	2.88
K_2O	0.80	0.44	0.57	0.58	0.52	0.37
P_2O_5	0.23	0.17	0.13	0.26	0.15	0.12
H_2O+	1.59	1.99	1.07	1.46	1.46	1.26
Total	100.04	99.78	99.80	99.94	99.51	99.43
D.I.	40.30	36.70	40.70	48.00	34.90	29.60
Nb	6	6	6	6	16	5
Be	1.00	n.d.	0.97	0.96	0.60	0.87
Zr	136	127	143	169	90	72
Y	27	21	25	29	16	15
Ba	214	198	212	220	101	130
Sr	351	403	357	336	274	245
Rb	11	7	8	11	10	8
Li	4	3	4	2	2	3
Hf	3.53	n.d.	3.67	4.33	3.50	1.96
Ta	0.15	n.d.	0.10	0.32	1.20	0.28
Th	5.17	n.d.	4.76	6.32	2.55	5.15
U	0.27	n.d.	0.42	0.65	0.16	0.47
Ga	15	16	15	15	12	12
Zn	81	84	75	75	83	88
Cu	10	15	13	14	12	14
Co	9	26	13	< 3	6	33
V	236	234	231	140	148	264
Ni	14	16	< 3	< 3	19	28
Cr	< 6	7	< 6	< 6	27	296
Sc	33	29	34	23	22	39
DF	121	137	170	256	310	180
La	21.30	n.d.	22.30	19.10	11.90	9.80
Ce	41.50	n.d.	42.80	35.00	28.10	19.00
Pr	5.57	n.d.	5.93	5.04	3.98	2.70
Nd	23.70	n.d.	24.90	20.90	18.20	11.20
Sm	5.62	n.d.	5.87	4.65	4.60	2.89
Eu	1.61	n.d.	1.73	1.31	1.49	0.87
Gd	6.33	n.d.	6.24	5.10	4.98	3.36
Tb	0.90	n.d.	0.90	0.70	0.64	0.47
Dy	5.92	n.d.	5.51	4.59	3.77	3.23
Ho	1.25	n.d.	1.18	1.00	0.69	0.69
Er	3.59	n.d.	3.44	3.01	1.80	2.05
Tm	0.54	n.d.	0.50	0.44	0.23	0.31
Yb	3.20	n.d.	3.19	2.52	1.25	1.95
Lu	0.49	n.d.	0.47	0.39	0.18	0.29